

# Quantum theory for the dynamic microstructure in correlated two-component systems far from equilibrium – Application to x-ray scattering

J. Vorberger<sup>1,2,\*</sup> and D.A. Chapman<sup>3,4</sup>

<sup>1</sup>*Max-Planck-Institute for the Physics of Complex System, D-01187 Dresden, Germany*

<sup>2</sup>*Institute of Radiation Physics, Helmholtz-Zentrum Dresden-Rossendorf e.V., D-01328 Dresden, Germany*

<sup>3</sup>*AWE plc, Aldermaston, Reading RG7 4PR, UK*

<sup>4</sup>*Centre for Fusion, Space and Astrophysics, University of Warwick, Coventry CV4 7AL, UK*

(Dated: January 25, 2016)

We present a quantum theory for the dynamic structure factors in non-equilibrium, correlated, two-component systems such as plasmas or warm dense matter. Using this general framework, we derive expressions for effective local field corrections to the random phase approximation. The polarization function, which is needed as the input for the calculation of the structure factors, is calculated in non-equilibrium based on a perturbation expansion in the interaction strength. To make our theory applicable for x-ray scattering, a generalized Chihara decomposition for the total electron structure factor in non-equilibrium is derived. Examples are given for the special case of equilibrium and for a model bump-on-hot-tail distribution, as often encountered during laser heating of materials.

PACS numbers: 52.27.Gr, 52.25.Mq, 52.70.La, 03.65.Nk

## I. INTRODUCTION

There exist many experimental methods to create and diagnose states of matter usually only found in the interior of planets or stars [1–4]. Such states feature a high energy density and are highly transient in the laboratory. The usual methods for creating such extreme states of matter involve the deposition of large amounts of energy into the system on time scales of femto- to pico- or nanoseconds. Apart from fundamental research and laboratory astrophysics, there are many applications of these methods in fields from medical therapy to industrial processes [5–8].

Inevitably, highly non-equilibrium states are produced. For instance, shock waves will heat the ions, initially leaving the electrons in the ground state [9–11]. On the other hand, using high-energy sources of electromagnetic or particle radiation, e.g. optical or x-ray lasers or ion beams, promotes the electrons to high-energy states whilst initially leaving the ions in the ground state, e.g. the lattice configuration of the undriven target [12–18]. Such systems have been modeled using a variety of numerical techniques including kinetic equations, particle-in-cell simulations and hybrid-fluid models [19–26].

Such non-equilibrium states can be created in macroscopic volumes and are therefore characterized, not necessarily by large inhomogeneities or anisotropies, but by Wigner distribution functions [27] far from the equilibrium form. Once a strongly non-equilibrium state has been created, the relaxation of the system towards equilibrium involves many intricately linked and interesting processes like the build up of correlations, the formation of equilibrium (Fermi-shaped) distribution functions

within the electron and ion subsystems, ionization balance, as well as energy and temperature relaxation between species [24, 28–32]. In particular, current experiments combining high-power short-pulse optical lasers and x-ray free electron lasers (XFELs), to respectively create and probe warm dense matter, enable unprecedented insight into the complex microstructure of a variety of exotic states [3, 17, 33–35].

Spectrally or angularly resolving the probing radiation scattered by the sample provides a direct measurement of the total (bound and free) electronic structure factor. Such a setup provides an ideal platform for comparing experimental data to cutting edge theoretical models. By fitting experimental spectra with theoretical calculations, estimates of the plasma conditions, such as the ionization balance, density and mean energy (in thermal equilibrium this relates either to the temperature or the Fermi energy, depending on the importance of degeneracy), may be inferred in addition to the static and dynamic structure or information about collective modes [3, 11, 36–42]. Experiments using such x-ray Thomson scattering (XRTS) are therefore envisaged to shed light onto open problems in the understanding of the relaxation of particle momenta and energy and also temperature equilibration [9, 10, 18, 32, 43, 44].

While low lying bound state spectra have been investigated in non-equilibrium [45], state of the art theories for the calculation of the total electron structure and scattering spectrum are valid in equilibrium only and can be applied to two-temperature systems only in very special circumstances [46–54]. Until now, fully non-equilibrium calculations have been restricted to the weakly coupled electron gas [23, 55].

In this paper, we present a complete theoretical model which allows the study of non-equilibrium two-component systems beyond the random phase approximation (RPA) for the first time. Although we do not con-

---

\*Electronic address: j.vorberger@hzdr.de

sider inhomogeneous or anisotropic systems, we fully account for non-equilibrium Wigner distribution functions. The evolution of the distribution functions is assumed to be known from other means, such as the solution of kinetic equations or simulations [17, 19, 20]. In order to be able to analyze the scattered signal in non-equilibrium, we generalize the concept of the Chihara decomposition of the total electron structure factor. Approximations like the scale separation of electron and ion structure in energy (Born-Oppenheimer approximation) are avoided. For the important case of weak electron-ion coupling, generalized local field corrections are derived.

This paper is organized as follows: Section II contains the derivation of the dynamic structure factors for a correlated two-component quantum system in non-equilibrium. Then, section III shows a possible generalization of the concept of local field corrections for non-equilibrium while section IV presents the approximation for the input quantity polarization function and the contributing vertex and self energy terms. Section V presents results for the non-equilibrium and equilibrium structure and discusses these results. In section VI, a generalized Chihara formula for non-equilibrium is derived and expressions for the generalized screening cloud and free electron structure are presented. Examples for such a decomposition of the total structure are shown.

## II. THEORETICAL DESCRIPTION OF THE DYNAMIC STRUCTURE FACTOR FOR NON-EQUILIBRIUM SYSTEMS

The dynamic structure factor (DSF) contains information about the time dependent long- and short-range order of the system. Further, the occurrence and dispersion of collective excitations can be extracted from the DSF. The latter also gives information about the coupling of electrons and ions.

In a non-equilibrium system of particles obeying quantum statistics (such as fermions), the DSF is given by the correlation function of density fluctuations  $L^>$  [27, 56]

$$S_{ab}(\mathbf{p}, \omega; t) = \frac{1}{2\pi} \int d\mathbf{r} d\tau iL_{ab}^>(12) e^{-i\mathbf{p}\mathbf{r} + i\omega\tau}. \quad (1)$$

Here,  $\{a, b\} = \{e, i\}$  denotes the species of particles in the systems. The density fluctuations are given in position space by  $\delta\rho_a(1) = \psi_a^\dagger(1)\psi_a(1) - \langle\psi_a^\dagger(1)\psi_a(1)\rangle$  with  $1 = \{\mathbf{r}_1, t_1, \sigma_1\}$  and therefore  $iL_{ab}^>(12) = \langle\delta\rho_a(1)\delta\rho_b(2)\rangle$ . Here,  $\langle\ldots\rangle$  denotes the average with the non-equilibrium density operator. We have introduced center of mass and relative coordinates for time and space, i.e.,  $\tau = t_1 - t_2$  and  $t = \frac{1}{2}(t_1 + t_2)$  and  $\mathbf{r} = \mathbf{r}_1 - \mathbf{r}_2$ ,  $\mathbf{R} = \frac{1}{2}(\mathbf{r}_1 + \mathbf{r}_2)$ .

The macroscopic time evolution is contained in  $t$  and the macroscopic space dependence  $\mathbf{R}$  has been dropped. The Fourier transform is then performed over the microscopic time and space coordinates  $\tau$  and  $\mathbf{r}$ , respectively.

Expression (1) represents a general form of the well-known fluctuation-dissipation theorem. The function  $L_{ab}^>$  is defined in the particle-hole channel and is a special case of the function  $L_{ab}$ . The equation of motion for  $L_{ab}$  defined on the Keldysh time contour is given by [27, 57]

$$L_{ab}(t_1, t_2) = \Pi_{ab}(t_1, t_2) + \sum_{c,d} \int_{\mathcal{C}} dt_3 \Pi_{ac}(t_1, t_3) V_{cd} L_{db}(t_3, t_2). \quad (2)$$

Here,  $\Pi_{ab}$  is the polarization function, which determines the response of the particles to the mean field in the system  $\Pi_{ab}(12, 1'2') = \pm i\delta g_a(11')/\delta U_b^{\text{eff}}(2'2)$  [27].  $V_{ab}$  is the Coulomb potential acting between the particles, and the symbol  $\int_{\mathcal{C}}$  stands for the integration along the Keldysh contour. Only the time variables are given explicitly, an entire set of variables is  $1 = \{\mathbf{r}_1, t_1, \sigma_1\}$ . Equations for the correlation function  $L_{ab}^>$ , and for the retarded and advanced functions  $L_{ab}^{\text{R/A}}$  can be obtained from Eq. (2) using the Keldysh techniques [27, 57].

In this work, we limit the discussion to two-component (e.g. electron-ion) systems. Following the same general route as used in Vorberger et al. [32], we rewrite the system of equations generated by Eq. (2) as

$$\begin{aligned} L_{ee} &= \mathcal{L}_{ee} + \mathcal{R}_{ee} + (\mathcal{R}_{ee}V_{ee} + \mathcal{R}_{ei}V_{ie})L_{ee}, \\ L_{ii} &= \mathcal{L}_{ii} + \mathcal{R}_{ii} + (\mathcal{R}_{ii}V_{ii} + \mathcal{R}_{ie}V_{ei})L_{ii}, \\ L_{ei} &= \mathcal{L}_{ei} + \mathcal{R}_{ei} + (\mathcal{R}_{ei}V_{ie} + \mathcal{R}_{ee}V_{ee})L_{ei}, \\ L_{ie} &= \mathcal{L}_{ie} + \mathcal{R}_{ie} + (\mathcal{R}_{ie}V_{ei} + \mathcal{R}_{ii}V_{ii})L_{ie}. \end{aligned} \quad (3)$$

Here, we used a compact form suppressing all spatio-temporal variables and integrations, such that the equations have the same structure as Eq. (2). We introduced the correlation functions within a sub-system

$$\begin{aligned} \mathcal{L}_{aa} &= \Pi_{aa} + (\Pi_{aa}V_{aa} + \Pi_{ab}V_{ba})\mathcal{L}_{aa}, \\ \mathcal{L}_{ab} &= \Pi_{ab} + (\Pi_{aa}V_{aa} + \Pi_{ab}V_{ba})\mathcal{L}_{ab}, \end{aligned} \quad (4)$$

and defined additional functions which collect cross species correlations

$$\begin{aligned} \mathcal{R}_{aa} &= \mathcal{L}_{aa}V_{ab}\mathcal{L}_{ba} + \mathcal{L}_{ab}V_{bb}\mathcal{L}_{ba}, \\ \mathcal{R}_{ab} &= \mathcal{L}_{aa}V_{ab}\mathcal{L}_{bb} + \mathcal{L}_{ab}V_{bb}\mathcal{L}_{bb}. \end{aligned} \quad (5)$$

The structure of these equations is also similar to Eq. (2). Upon transferring from the contour to the physical time axis, the Langreth-Wilkins rules are used to obtain [58]

$$\begin{aligned}
L_{ee}^>(t_1, t_2) &= \mathcal{L}_{ee}^>(t_1, t_2) + \mathcal{R}_{ee}^>(t_1, t_2) + \int_{-\infty}^{+\infty} dt_3 [\mathcal{R}_{ee}^>(t_1, t_3) V_{ee} + \mathcal{R}_{ei}^>(t_1, t_3) V_{ie}] L_{ee}^A(t_3, t_2) \\
&+ \int_{-\infty}^{+\infty} dt_3 [\mathcal{R}_{ee}^R(t_1, t_3) V_{ee} + \mathcal{R}_{ei}^R(t_1, t_3) V_{ie}] L_{ee}^>(t_3, t_2)
\end{aligned} \tag{6}$$

Similarly, we obtain

$$\begin{aligned}
L_{ii}^> &= \mathcal{L}_{ii}^> + \mathcal{R}_{ee}^> + (\mathcal{R}_{ii}^> V_{ii} + \mathcal{R}_{ie}^> V_{ei}) L_{ii}^A \\
&+ (\mathcal{R}_{ii}^R V_{ii} + \mathcal{R}_{ie}^R V_{ei}) L_{ii}^>, \\
L_{ei}^> &= \mathcal{L}_{ei}^> + \mathcal{R}_{ei}^> + (\mathcal{R}_{ei}^> V_{ie} + \mathcal{R}_{ee}^> V_{ee}) L_{ei}^A \\
&+ (\mathcal{R}_{ei}^R V_{ie} + \mathcal{R}_{ee}^R V_{ee}) L_{ei}^>, \\
L_{ie}^> &= \mathcal{L}_{ie}^> + \mathcal{R}_{ie}^> + (\mathcal{R}_{ie}^> V_{ei} + \mathcal{R}_{ii}^> V_{ii}) L_{ie}^A \\
&+ (\mathcal{R}_{ie}^R V_{ei} + \mathcal{R}_{ii}^R V_{ii}) L_{ie}^>,
\end{aligned} \tag{7}$$

where the integration and its intervals are similar to Eq. (6). The subsystem equations (4) and the auxiliary quantities (5) follow as

$$\begin{aligned}
\mathcal{L}_{aa}^> &= \Pi_{aa}^> + (\Pi_{aa}^> V_{aa} + \Pi_{ab}^> V_{ba}) \mathcal{L}_{aa}^A \\
&+ (\Pi_{aa}^R V_{aa} + \Pi_{ab}^R V_{ba}) \mathcal{L}_{aa}^>, \\
\mathcal{L}_{ab}^> &= \Pi_{ab}^> + (\Pi_{aa}^> V_{aa} + \Pi_{ab}^> V_{ba}) \mathcal{L}_{ab}^A \\
&+ (\Pi_{aa}^R V_{aa} + \Pi_{ab}^R V_{ba}) \mathcal{L}_{ab}^>,
\end{aligned} \tag{8}$$

and

$$\begin{aligned}
\mathcal{R}_{aa}^> &= \mathcal{L}_{aa}^> V_{ab} \mathcal{L}_{ba}^A + \mathcal{L}_{aa}^R V_{ab} \mathcal{L}_{ba}^> \\
&+ \mathcal{L}_{ab}^> V_{bb} \mathcal{L}_{ba}^A + \mathcal{L}_{ab}^R V_{bb} \mathcal{L}_{ba}^>, \\
\mathcal{R}_{ab}^> &= \mathcal{L}_{aa}^> V_{ab} \mathcal{L}_{bb}^A + \mathcal{L}_{aa}^R V_{ab} \mathcal{L}_{bb}^> \\
&+ \mathcal{L}_{ab}^> V_{bb} \mathcal{L}_{bb}^A + \mathcal{L}_{ab}^R V_{bb} \mathcal{L}_{bb}^>.
\end{aligned} \tag{9}$$

The complimentary retarded and advanced quantities are

$$\begin{aligned}
L_{ee}^{R/A} &= \mathcal{L}_{ee}^{R/A} + \mathcal{R}_{ee}^{R/A} + (\mathcal{R}_{ee}^{R/A} V_{ee} + \mathcal{R}_{ei}^{R/A} V_{ie}) L_{ee}^{R/A}, \\
L_{ii}^{R/A} &= \mathcal{L}_{ii}^{R/A} + \mathcal{R}_{ii}^{R/A} + (\mathcal{R}_{ii}^{R/A} V_{ii} + \mathcal{R}_{ie}^{R/A} V_{ei}) L_{ii}^{R/A}, \\
L_{ei}^{R/A} &= \mathcal{L}_{ei}^{R/A} + \mathcal{R}_{ei}^{R/A} + (\mathcal{R}_{ei}^{R/A} V_{ie} + \mathcal{R}_{ee}^{R/A} V_{ee}) L_{ei}^{R/A}, \\
L_{ie}^{R/A} &= \mathcal{L}_{ie}^{R/A} + \mathcal{R}_{ie}^{R/A} + (\mathcal{R}_{ie}^{R/A} V_{ei} + \mathcal{R}_{ii}^{R/A} V_{ii}) L_{ie}^{R/A},
\end{aligned} \tag{10}$$

and

$$\begin{aligned}
\mathcal{L}_{aa}^{R/A} &= \Pi_{aa}^{R/A} + (\Pi_{aa}^{R/A} V_{aa} + \Pi_{ab}^{R/A} V_{ba}) \mathcal{L}_{aa}^{R/A}, \\
\mathcal{L}_{ab}^{R/A} &= \Pi_{ab}^{R/A} + (\Pi_{aa}^{R/A} V_{aa} - \Pi_{ab}^{R/A} V_{ba}) \mathcal{L}_{ab}^{R/A},
\end{aligned} \tag{11}$$

as well as

$$\begin{aligned}
\mathcal{R}_{aa}^{R/A} &= \mathcal{L}_{aa}^{R/A} V_{ab} \mathcal{L}_{ba}^{R/A} + \mathcal{L}_{ab}^{R/A} V_{bb} \mathcal{L}_{ba}^{R/A}, \\
\mathcal{R}_{ab}^{R/A} &= \mathcal{L}_{aa}^{R/A} V_{ab} \mathcal{L}_{bb}^{R/A} + \mathcal{L}_{ab}^{R/A} V_{bb} \mathcal{L}_{bb}^{R/A}.
\end{aligned} \tag{12}$$

We now introduce center of mass and relative coordinates. In non-equilibrium, the macroscopic variables  $t$  and  $\mathbf{R}$  are coupled with the microscopic variables  $\tau$  and  $\mathbf{r}$  [27]. However, in local approximation, i.e. in lowest order gradient expansion, these spatio-temporal scales are formally decoupled, thereby enabling Fourier transformations to be taken with respect to the relative variables  $\mathbf{r}$  and  $\tau$  [27]. Naturally, if the non-equilibrium system is considered to be spatially homogeneous, all dependencies on  $\mathbf{R}$  vanish. The set of equations (6) has the structure of a convolution in real space and, thus, becomes algebraic in momentum-frequency space.

After some lengthy algebra, the result for the electronic density fluctuation correlation function is found to be

$$L_{ee}^> = \frac{\mathcal{Q}_{ee}^>(1 - \mathcal{T}_{ee}^A) + \mathcal{T}_{ee}^> \mathcal{Q}_{ee}^A}{|1 - \mathcal{T}_{ee}^R|^2}, \tag{13}$$

where all functions now depend on the set of Fourier variables  $\mathbf{p}, \omega$  and the macroscopic time  $t$ , i.e.  $L_{ee}^> \equiv L_{ee}^>(\mathbf{p}, \omega; t)$ . In Eq. (13), we have also defined

$$\begin{aligned}
\mathcal{Q}_{ab}^X &= \mathcal{L}_{ab}^X + \mathcal{R}_{ab}^X, \\
\mathcal{T}_{ee}^X &= V_{ee} \mathcal{R}_{ee}^X + V_{ie} \mathcal{R}_{ei}^X, \\
\mathcal{T}_{ii}^X &= V_{ii} \mathcal{R}_{ii}^X + V_{ei} \mathcal{R}_{ie}^X,
\end{aligned} \tag{14}$$

where X stands for R/A or  $\geq$ , as required. Again, all quantities depend on the variables  $\{\mathbf{p}, \omega, t\}$ , except the Coulomb potential  $V_{ab} \equiv V_{ab}(p)$ . The complexity of this structure is the result of the interplay of correlations within and between the distinct subsystems.

Considering only diagonal elements to the polarization function, i.e.  $\Pi_{ei} = \Pi_{ie} = 0$ , one straightforwardly finds  $\mathcal{L}_{ab} = 0$  and subsequently  $\mathcal{R}_{aa} = \mathcal{R}_{bb} = 0$ . Under this diagonalized polarization approximation (DPA), Eq. (13) becomes

$$L_{ee}^> = \frac{\mathcal{L}_{ee}^> + |\mathcal{L}_{ee}^R|^2 V_{ei}^2 \mathcal{L}_{ii}^>}{|1 - V_{ie} \mathcal{L}_{ee}^R V_{ei} \mathcal{L}_{ii}^R|^2}. \tag{15}$$

In this case, the direct electron-ion coupling is weak and a visualization of the physics within a two fluid picture is appropriate. The first term in the numerator of Eq. (15) is the pure electron gas contribution [23]. It is followed by the ionic structure contributions to the total electronic structure (via the electronic screening cloud). The electronic and ionic systems are coupled via the denominator. An example of the effects of this coupling is

given by the screening of the ionic plasmon mode that produces the ion acoustic density oscillations [32, 59].

The other correlation functions of interest read

$$L_{ei}^> = \frac{\mathcal{Q}_{ei}^>(1 - \mathcal{T}_{ee}^A) + \mathcal{T}_{ee}^>\mathcal{Q}_{ei}^A}{|1 - \mathcal{T}_{ee}^R|^2}, \quad (16)$$

$$L_{ii}^> = \frac{\mathcal{Q}_{ii}^>(1 - \mathcal{T}_{ii}^A) + \mathcal{T}_{ii}^>\mathcal{Q}_{ii}^A}{|1 - \mathcal{T}_{ii}^R|^2}, \quad (17)$$

$$L_{ie}^> = \frac{\mathcal{Q}_{ie}^>(1 - \mathcal{T}_{ii}^A) + \mathcal{T}_{ii}^>\mathcal{Q}_{ie}^A}{|1 - \mathcal{T}_{ii}^R|^2}. \quad (18)$$

We again give the interesting case of the DPA

$$L_{ei}^> = \frac{\mathcal{R}_{ei}^>}{|1 - V_{ie}\mathcal{L}_{ee}^R V_{ei}\mathcal{L}_{ii}^R|^2}, \quad (19)$$

$$L_{ii}^> = \frac{\mathcal{L}_{ii}^> + |\mathcal{L}_{ii}^R|^2 V_{ie}^2 \mathcal{L}_{ee}^>}{|1 - V_{ie}\mathcal{L}_{ee}^R V_{ei}\mathcal{L}_{ii}^R|^2}, \quad (20)$$

$$L_{ie}^> = \frac{\mathcal{R}_{ie}^>}{|1 - V_{ie}\mathcal{L}_{ee}^R V_{ei}\mathcal{L}_{ii}^R|^2}. \quad (21)$$

Note that the expression for  $L_{ei}^>$  (19) corresponds to the one derived for the electron-ion energy transfer rate by Vorberger *et al.* [32]. Accordingly, the exact expression (16) offers more channels for the energy transfer then considered in energy transfer rates used so far.)

The task is now to calculate the correlation functions and retarded functions for the sub-systems, e.g.

$$\begin{aligned} \mathcal{L}_{aa}^> &= \frac{\Pi_{aa}^>(1 - V_{ba}\Pi_{ab}^A) + \Pi_{aa}^A V_{ba}\Pi_{ab}^>}{|1 - V_{aa}\Pi_{aa}^R - V_{ba}\Pi_{ab}^R|^2}, \\ \mathcal{L}_{ab}^> &= \frac{\Pi_{ab}^>(1 - V_{aa}\Pi_{aa}^A) + \Pi_{ab}^A V_{aa}\Pi_{aa}^>}{|1 - V_{aa}\Pi_{aa}^R - V_{ba}\Pi_{ab}^R|^2}, \end{aligned} \quad (22)$$

and

$$\begin{aligned} \mathcal{L}_{aa}^{R/A} &= \frac{\Pi_{aa}^{R/A}}{1 - V_{aa}\Pi_{aa}^{R/A} - V_{ba}\Pi_{ab}^{R/A}}, \\ \mathcal{L}_{ab}^{R/A} &= \frac{\Pi_{ab}^{R/A}}{1 - V_{aa}\Pi_{aa}^{R/A} - V_{ba}\Pi_{ab}^{R/A}}. \end{aligned} \quad (23)$$

Again, the subscripts  $a = \{e, i\}$  and  $b = \{e, i\}$  denote the ions and electrons, respectively. The  $\mathcal{L}_{aa}$  become true one species correlation functions in the DPA wherein one has  $\mathcal{L}_{ab} = 0$ .

### III. THE DYNAMIC LOCAL FIELD CORRECTION IN NON-EQUILIBRIUM SYSTEMS

In equilibrium situations, correlations beyond the RPA are often accounted for via local field corrections (LFC)  $G(\mathbf{p}, \omega)$  [47, 49, 52, 60–63]. LFCs are introduced in equilibrium to deliver the true density fluctuation correlation

function via the ansatz

$$\begin{aligned} L(\mathbf{p}, \omega) &= \frac{\Pi(\mathbf{p}, \omega)}{1 - V(\mathbf{p}) \Pi(\mathbf{p}, \omega)} \\ &\stackrel{!}{=} \frac{L^0(\mathbf{p}, \omega)}{1 - V(\mathbf{p}) [1 - G(\mathbf{p}, \omega)] L^0(\mathbf{p}, \omega)}. \end{aligned} \quad (24)$$

Although a structure such as Eq. (24) is straightforward to realize in equilibrium, wherein only retarded quantities are required, a different framework is required under non-equilibrium conditions. In particular, a connection in the realm of the microscopic time variables instead of in frequency space is required in order to properly account for the time ordering that underpins the correlation functions. An exact equation of motion for the density fluctuation correlation function in terms of the free density response  $L^0$  usually contains at least a three point function for which the time ordering cannot be established easily [27].

For the purposes of this work, we assume that a structure similar to Eq. (24) can be introduced to deal with correlations beyond RPA in non-equilibrium. Thus, we seek to establish the appropriate time ordering for such a term and subsequently develop a generalized LFC. Note that this is not strictly necessary once a better approximation for the polarization functions in non-equilibrium can be obtained. We will also consider the DPA only and, thus, restrict ourselves to conditions with weak direct electron-ion coupling. This is in the spirit of all the methods for LFCs in equilibrium, which are usually derived for one-component systems. Therefore, we assume this structure in the time domain:

$$\begin{aligned} \mathcal{L}_{aa}(t_1, t_2) &= \mathcal{L}_{aa}^0(t_1, t_2) \\ &+ \int_{\mathcal{C}} dt_3 dt_4 \mathcal{L}_{aa}^0(t_1, t_3) \Xi_{aa}(t_3, t_4) \mathcal{L}_{aa}(t_4, t_2), \end{aligned} \quad (25)$$

in which  $\Xi_{aa}(t_3, t_4) = V_{aa}[1 - G_{aa}(t_3, t_4)]$  and  $\mathcal{L}_{aa}^0$  is the density response function of a non-interacting system. The latter and its correlation functions are given by the RPA expression for the polarization function Eq. (35). As before, the integral has a convolution structure only in local approximation. Applying the Langreth-Wilkins rules once more, the result in Fourier space (again suppressing all variables  $\{\mathbf{p}, \omega, t\}$ ) is

$$\mathcal{L}_{aa}^> = \frac{\mathcal{L}_{aa}^{0>} - V_{aa}G_{aa}^>|\mathcal{L}_{aa}^{0R}|^2}{|1 - V_{aa}[1 - G_{aa}^R]\mathcal{L}_{aa}^{0R}|^2}, \quad (26)$$

for the density fluctuation correlation function of a correlated species. For the retarded density correlation function follows a familiar expression

$$\mathcal{L}_{aa}^R = \frac{\mathcal{L}_{aa}^{0R}}{1 - V_{aa}[1 - G_{aa}^R]\mathcal{L}_{aa}^{0R}}. \quad (27)$$

The difference to the equilibrium expression Eq. (24) lies in the time dependence given by the changing non-equilibrium distribution functions entering the calculations. From Eqs. (27) & (11), there immediately follows

a general expression for the retarded local field correction in non-equilibrium systems

$$G_{aa}^R(\mathbf{p}, \omega; t) = \frac{1}{V_{aa}(\mathbf{p})} \left\{ \frac{1}{\Pi_{aa}^R(\mathbf{p}, \omega; t)} - \frac{1}{\mathcal{L}_{aa}^{0R}(\mathbf{p}, \omega; t)} \right\}. \quad (28)$$

Using this expression in Eq. (26) and comparing with Eq. (8), the correlation function  $G^>$  for the LFC is

$$G_{aa}^>(\mathbf{p}, \omega; t) = \frac{1}{V_{aa}(\mathbf{p})} \left\{ \frac{\mathcal{L}_{aa}^{0>}(\mathbf{p}, \omega; t)}{|\mathcal{L}_{aa}^{0R}(\mathbf{p}, \omega; t)|^2} - \frac{\Pi_{aa}^>(\mathbf{p}, \omega; t)}{|\Pi_{aa}^R(\mathbf{p}, \omega; t)|^2} \right\}. \quad (29)$$

Such expressions are not very useful in non-equilibrium systems since closure relations that connect the LFCs to the dynamic structure factor as in equilibrium, e.g. Ref. [60], do not exist so far. Furthermore, in general, one needs two relations since the correlation function of the LFC  $G^>$  and the retarded LFC  $G^R$  are not easily connected in non-equilibrium.

It is nevertheless interesting to observe that these relations reduce to the well known formulas for equilibrium systems. In this case, the spectral representation of the correlation functions leads to [27]

$$\mathcal{L}_{aa}^{0>}(\mathbf{p}, \omega) = -2[1 + n_B(\omega)] \text{Im} \mathcal{L}_{aa}^R(\mathbf{p}, \omega), \quad (30)$$

$$\Pi_{aa}^>(\mathbf{p}, \omega) = -2[1 + n_B(\omega)] \text{Im} \Pi_{aa}^R(\mathbf{p}, \omega). \quad (31)$$

The Bose function is given by  $n_B(\omega) = [\exp(\beta\omega) - 1]^{-1}$  with  $\beta^{-1} = k_B T$ . This produces a similar spectral representation for the LFCs

$$G_{aa}^>(\mathbf{p}, \omega) = -2[1 + n_B(\omega)] \text{Im} G_{aa}^R(\mathbf{p}, \omega). \quad (32)$$

Inserting this expression into Eq. (26) gives the familiar result for the density fluctuations

$$i\mathcal{L}_{aa}^>(\mathbf{p}, \omega) = -2[1 + n_B(\omega)] \frac{\text{Im} \mathcal{L}_{aa}^{0R}(\mathbf{p}, \omega) - V_{aa}(\mathbf{p}) \text{Im} G_{aa}^R(\mathbf{p}, \omega) |\mathcal{L}_{aa}^{0R}(\mathbf{p}, \omega)|^2}{\left| 1 - V_{aa}(\mathbf{p}) [1 - G_{aa}^R(\mathbf{p}, \omega)] \mathcal{L}_{aa}^{0R}(\mathbf{p}, \omega) \right|^2}, \quad (33)$$

and also the familiar expression for the dynamic structure factor once Eqs. (1) & (13) are used.

#### IV. APPROXIMATION FOR THE POLARIZATION FUNCTION IN NON-EQUILIBRIUM SYSTEMS

The equations of motion derived in the preceding sections show that the total density fluctuations, and therefore the total structure, are given by a sum over local density fluctuations excited by the effective field in the system and described by the polarization function.

Since a self-consistent approach to the polarization function for correlated, non-equilibrium systems is currently not possible, we evaluate correlation effects beyond

RPA by establishing a perturbation series. In particular, we retain the exact first order corrections which account for self energy and exchange. Such a method has been used before to various perturbation orders including even the full vertex function [64–72]. However, all these calculations have been performed for equilibrium systems which simplifies things considerably. Further, as we are motivated by current experiments producing and studying warm dense matter, we need dynamic corrections to RPA for a broad parameter space including degenerate and non-degenerate systems of high density.

To this end, we consider two terms in addition to the RPA polarization function [27, 73]

$$\Pi_{ab} = \delta_{ab} \cdot (2\sigma_a + 1) \cdot (\Pi_a^{\text{RPA}} + \Pi_a^{\text{S}} + \Pi_a^{\text{V}}). \quad (34)$$

The first additional term is the self energy correction  $\Pi_a^{\text{S}}$ , which is given by two topologically identical terms  $\Pi_a^{S0}$  in lowest order but may also include higher order self energy correction by way of the Dyson equation. The second term is the vertex correction  $\Pi_a^{\text{V}}$ . We also include the spin contribution of all terms.

This series expansion contains all first order terms. At second order, one finds ten terms, eight of which correspond to self energy or vertex corrections (or combinations of the two), which are also all single species terms similar to Eq. (34). The remaining two second order terms are the first to account for inter-species correlations. This may explain the fact that the two fluid approach with neglected direct electron-ion polarization functions is so successful in describing many systems. Further, as inter-species terms are all of second order or higher, it is unlikely that a perturbative treatment of these will be sufficient and a full summation of the ladder is required once electron-ion correlations become important.

#### A. Random Phase Approximation

The RPA term has been considered in non-equilibrium before [23]. We give the correlation functions of the RPA contribution for completeness

$$\Pi_a^{\text{RPA}} \gtrless(1, 2) = -i\hbar g_a^{\gtrless}(1, 2) g_a^{\lesseqgtr}(2, 1). \quad (35)$$

We now switch to center of mass and relative coordinates and perform a Fourier transform with respect to the microscopic variables  $\mathbf{r}$  and  $\tau$ . Then we use the Kadanoff-Baym Ansatz, a generalization of the spectral representation for Green's functions in equilibrium, to write [27]

$$g_a^{\gtrless}(\mathbf{p}, \omega; t) = 2\pi i \delta(\hbar\omega - E_a(\mathbf{p}, t)) f_a^{\gtrless}(\omega, t), \quad (36)$$

$$f_a^{\gtrless}(\omega, t) = \begin{cases} f_a(\omega, t) & \gtrless \rightarrow < \\ -[1 - f_a(\omega, t)] & \gtrless \rightarrow > \end{cases}. \quad (37)$$

The single-particle quasi energies are given by  $E_a(\mathbf{p}, t) = p^2/2m_a + \text{Re}\Sigma_a(\mathbf{p}, \omega; t)$ . In RPA, only free-particle dispersion relations are considered, such that the self energy term is neglected and we may write  $f_a^{\gtrless}(\mathbf{p}, t) \equiv$

$f_a^{\geq}(E_a(\mathbf{p}), t)$ . The result for the correlation functions in RPA is then straightforwardly found to be [23, 27]

$$\Pi_a^{\text{RPA}\geq}(\mathbf{p}, \omega; t) = -2\pi i \int \frac{d\mathbf{q}}{(2\pi\hbar)^3} f_a^{\geq}(\mathbf{p} + \mathbf{q}, t) f_a^{\leq}(\mathbf{q}, t) \times \delta(\hbar\omega - E_a(\mathbf{p} + \mathbf{q}) + E_a(\mathbf{q})). \quad (38)$$

Once the correlation functions are known, the retarded quantities may be obtained via the general Kramers-Kronig relationship [27]

$$\Pi_a^{\text{R}}(\mathbf{p}, \omega; t) = i \int_{-\infty}^{\infty} \frac{d\omega'}{2\pi} \frac{\Pi_a^{\geq}(\mathbf{p}, \omega'; t) - \Pi_a^{\leq}(\mathbf{p}, \omega'; t)}{\omega - \omega' + i\epsilon}. \quad (39)$$

with a positive  $\epsilon \rightarrow 0^+$ . The explicit result is [27]

$$\Pi_a^{\text{R}}(\mathbf{p}, \omega; t) = \int \frac{d\mathbf{q}}{(2\pi\hbar)^3} \frac{f_a(\mathbf{q}, t) - f_a(\mathbf{p} + \mathbf{q}, t)}{\hbar\omega + i\epsilon + E_a(\mathbf{q}) - E_a(\mathbf{q} + \mathbf{p})}, \quad (40)$$

The complex expression (40) can be split into its constituent real and imaginary parts using the well-known formula of Dirac-Plemlj [27].

## B. Vertex Correction

The vertex correction to the polarization function in Eq. (34) is of first order in the interaction and describes exchange. It reads [74]

$$\Pi_a^{\text{V}}(1, 2) = \hbar^2 \int_{\mathcal{C}} d3d4 g_a(1, 3) g_a(3, 2) V_{aa}^{\text{sc}}(3, 4) g_a(2, 4) g_a(4, 1). \quad (41)$$

In lowest order, the screened interaction  $V_{aa}^{\text{sc}}$  can be taken to be local in time

$$V_{aa}^{\text{sc}}(3, 4) = V_{aa}^{\text{sc}}(\mathbf{r}_3, \mathbf{r}_4) \delta(t_3 - t_4). \quad (42)$$

For instance, this is fulfilled by a statically screened interaction such as the Debye or FWS potentials [42]. Note that the convergence of this term does not depend on screening (a bare Coulomb potential is sufficient too) because the term describes exchange and is limited to short range only. In equation of state theory, this term is responsible for the appearance of the normal  $e^4$ -exchange term [73].

Using the locality of the potential in time, we write

$$\Pi_a^{\text{V}}(1, 2) = \hbar^2 \int d\mathbf{r}_3 d\mathbf{r}_4 V_{aa}^{\text{sc}}(\mathbf{r}_3, \mathbf{r}_4) \times \int_{\mathcal{C}} dt_3 \mathcal{G}_{13,41}(t_1, t_3) \mathcal{G}_{32,24}(t_3, t_2), \quad (43)$$

with  $\mathcal{G}_{13,41}(t_1, t_3) = g_a(\mathbf{r}_1 t_1, \mathbf{r}_3 t_3) g_a(\mathbf{r}_4 t_3, \mathbf{r}_1 t_1)$  and similarly for  $\mathcal{G}_{32,24}(t_3, t_2)$ . The transition from the Keldysh contour onto the physical time axis is once more performed using the Langreth-Wilkins rules. We also introduce again relative and center of mass coordinates in space and time. Then, a Fourier transform with respect to the microscopic variables is performed and the dependence on the center of mass coordinate is dropped. The result for the vertex term is

$$\Pi_a^{\text{V}\geq}(\mathbf{p}, \omega; t) = -2\hbar^2 \int_{-\infty}^{\infty} \frac{d\omega' d\omega'' d\omega'''}{(2\pi)^3} \frac{1}{\omega - \omega'} \mathcal{P} \int \frac{d\mathbf{k}' d\mathbf{k}''}{(2\pi\hbar)^6} V_{aa}^{\text{sc}}(\mathbf{k}' - \mathbf{k}'') g_a^{\geq}(\mathbf{k}', \omega + \omega'''; t) g_a^{\leq}(\mathbf{k}' + \mathbf{p}, \omega'''; t) \times [g_a^{\geq}(\mathbf{k}'', \omega' + \omega''; t) g_a^{\leq}(\mathbf{k}'' + \mathbf{p}, \omega''; t) - g_a^{\leq}(\mathbf{k}'', \omega' + \omega''; t) g_a^{\geq}(\mathbf{k}'' + \mathbf{p}, \omega''; t)]. \quad (44)$$

Here,  $\mathcal{P}$  denotes a Cauchy principal value integration. The single-particle correlation functions are then substituted via Eq. (36) and the result is

$$\Pi_a^{\text{V}\geq}(\mathbf{p}, \omega; t) = -4\pi \mathcal{P} \int \frac{d\mathbf{k}' d\mathbf{k}''}{(2\pi\hbar)^6} V_{aa}^{\text{sc}}(\mathbf{k}' - \mathbf{k}'') f_a^{\leq}(\mathbf{k}' + \mathbf{p}, t) f_a^{\geq}(\mathbf{k}', t) [f_a(\mathbf{k}'' + \mathbf{p}, t) - f_a(\mathbf{k}'', t)] \times \frac{\delta(E_a(\mathbf{k}' + \mathbf{p}) - E_a(\mathbf{k}') - \hbar\omega)}{E_a(\mathbf{k}'' + \mathbf{p}) - E_a(\mathbf{k}'') - \hbar\omega}. \quad (45)$$

It holds that  $f_a(\mathbf{p}, t) \equiv f_a^{\leq}(\mathbf{p}, t)$ . The corresponding expression for the retarded function follows from Eq. (39)

$$\Pi_a^{\text{V}\text{R}}(\mathbf{p}, \omega; t) = - \int \frac{d\mathbf{k}' d\mathbf{k}''}{(2\pi\hbar)^6} V_{aa}^{\text{sc}}(\mathbf{k}' - \mathbf{k}'') \frac{f_a(\mathbf{k}' + \mathbf{p}, t) - f_a(\mathbf{k}', t)}{\hbar\omega + i\epsilon + E_a(\mathbf{k}') - E_a(\mathbf{k}' + \mathbf{p})} \frac{f_a(\mathbf{k}'' + \mathbf{p}, t) - f_a(\mathbf{k}'', t)}{\hbar\omega + i\epsilon + E_a(\mathbf{k}'') - E_a(\mathbf{k}'' + \mathbf{p})}. \quad (46)$$

Note that an expression identical in form was obtained in equilibrium via the imaginary time Matsubara technique by DeWitt *et al.* [74].

We prefer to numerically evaluate the correlation functions of the vertex term (45) and then use the Kramers-Kronig relation (39) on the numerical data to obtain the retarded quantities instead of using Eq. (46) directly. In order to do so, we can reduce the number of integrations to be performed numerically in Eq. (45) from six to three

$$\begin{aligned} \Pi_a^{V\gtrless}(\mathbf{p}, \omega; t) = & i \frac{Z_a^2 e^2 m_a}{p \pi^2} \int_{\alpha}^{\infty} dk_1 k_1 \int_0^{\infty} dk_2 k_2^2 \mathcal{P} \int_{-1}^1 dx_2 \frac{f_a^{\leq}(k_1, t) f_a^{\geq}(\sqrt{k_1^2 + p^2 - 2k_1 p x_0}, t)}{\sqrt{|r^2 - s^2|}} \\ & \times \frac{f_a(\sqrt{k_2^2 + p^2 - 2k_2 p x_2}, t) - f_a(k_2, t)}{\frac{k_2 p x_2}{m_a} - \frac{p^2}{2m_a} + \hbar\omega}. \end{aligned} \quad (47)$$

Here,  $m_a$  is the mass of the species particles,  $Z_a$  the charge, and  $e$  the elementary charge. The summands  $r$  and  $s$  in the denominator of the second line are functions of the integration variables

$$r = k_1^2 + k_2^2 - k_1 k_2 x_0 x_2, \quad (48)$$

$$s = \sqrt{(1 - x_0^2)(1 - x_2^2)}, \quad (49)$$

$$x_0 = \frac{m_a}{k_1 p} \left( \frac{p^2}{2m_a} - \hbar\omega \right). \quad (50)$$

The lower limit  $\alpha$  of the momentum integration  $k_1$  is given by the condition  $-1 \leq x_0 \leq 1$ . We use three nested adaptive Gaussian quadratures for the numerical evaluation of this term. For the principal value integration in  $x_2$ , an adaptive Gaussian quadrature is used that picks the integration points symmetrically around the pole. The singularity for  $r^2 = s^2$  is integrable and

division by zero is avoided by adding  $\eta = 10^{-6}$  under the square root in the denominator.

### C. Self Energy Corrections

Self energy corrections in the series (34) can be introduced via the Dyson equation. The first term is the Hartree-Fock (HF) contribution [27]

$$\Pi_a^{S\gtrless}(1, 2) = -i\hbar g_a^{\text{HF}\gtrless}(1, 2) g_a^{\text{HF}\lesseqgtr}(2, 1). \quad (51)$$

This equation of course includes the RPA contribution in Eq. (34) and has to be used instead of Eq. (35) not in addition to it. The evaluation proceeds analogously to the RPA case and the final expression is

$$\Pi_a^{S\gtrless}(\mathbf{p}, \omega; t) = -2\pi i \int \frac{d\mathbf{q}}{(2\pi\hbar)^3} \delta(\hbar\omega - E_a^{\text{HF}}(\mathbf{p} + \mathbf{q}, t) + E_a^{\text{HF}}(\mathbf{q}, t)) f_a^{\geq}(E_a^{\text{HF}}(\mathbf{p} + \mathbf{q}, t)) f_a^{\leq}(E_a^{\text{HF}}(\mathbf{q} + \mathbf{p}) - \hbar\omega, t), \quad (52)$$

where the single-particle energies are now given by

$$E_a^{\text{HF}}(p, t) = \frac{p^2}{2m_a} + \Sigma_a^{\text{HF}}(p, t), \quad (53)$$

with the Hartree-Fock self energy to be calculated from

$$\begin{aligned} \Sigma_a^{\text{HF}}(p, t) &= - \int \frac{d\mathbf{q}}{(2\pi\hbar)^3} V_{aa}(\mathbf{p} - \mathbf{q}) f_a(\mathbf{q}, t), \\ &= - \frac{Z_a^2 e^2}{\pi p} \int_0^{\infty} q dq f_a(q, t) \ln \left| \frac{q + p}{q - p} \right|. \end{aligned} \quad (54)$$

Again, the perturbation expansion for the polarization function (34) contains a screened potential in the self energy. The lowest order of the latter is of course a bare Coulomb interaction whose use here does not lead to divergences as the HF self energy term is due to exchange and is therefore naturally restricted to small distances.

We may choose to insert a screened potential local in time, e.g. a statically screened potential, although a consistent perturbation expansion makes use of a Coulomb potential.

This expression for the self energy correction (51) is not of lowest order and problems with the f-sum rule and particle number conservation can occur. However, it is a convenient self energy correction to calculate that obeys the relation  $\Pi_a^>(\mathbf{p}, -\omega; t) = \Pi_a^<(\mathbf{p}, \omega; t)$  which is essential for a proper description of detailed balance in equilibrium and the spectrum of the scattering signal.

For consistency and comparison with known expressions, we give the lowest order self energy corrections to the RPA polarization function [74]

$$\begin{aligned} \Pi_a^{S0}(1, 2) &= \\ & \hbar^2 \int d3d4 g_a(1, 3) g_a(3, 4) V_{aa}^{\text{sc}}(3, 4) g_a(4, 2) g_a(2, 1). \end{aligned} \quad (55)$$

This is one of two topologically identical terms which, in equilibrium, give equal contributions to the total first order self energy correction. In non-equilibrium, we have to separately evaluate both terms.

We present the evaluation of just one term since the calculation of the other one proceeds similarly. The transformation into momentum-frequency space is similar as for the RPA term once we rewrite the (extended) self energy terms as

$$\Pi_a^{\text{SX}}(1, 2) = -i\hbar g_a^{\text{HF}}(1, 2)g_a(2, 1) - \Pi_a^{\text{RPA}}(1, 2), \quad (56)$$

---


$$\Pi_a^{\text{SX}\gtrless}(\mathbf{p}, \omega; t) = -2\pi i \int \frac{d\mathbf{q}}{(2\pi\hbar)^3} f_a^{\gtrless}(\mathbf{q} + \mathbf{p}, t) f_a^{\lesseqgtr}(E_a(\mathbf{q} + \mathbf{p}) - \hbar\omega, t) \delta(\hbar\omega + E_a^{\text{HF}}(\mathbf{q}, t) - E_a(\mathbf{q} + \mathbf{p})) - \Pi_a^{\text{RPA}\gtrless}(\mathbf{p}, \omega; t). \quad (57)$$


---

The retarded self energy correction to the polarization functions follows via Kramers-Kronig relation

$$\Pi_a^{\text{SX}^{\text{R}}}(\mathbf{p}, \omega; t) = \int \frac{d\mathbf{q}}{(2\pi\hbar)^3} \frac{f_a(\mathbf{q} + \mathbf{p}, t) - f_a(E_a^{\text{HF}}(\mathbf{q}, t))}{E_a(\mathbf{q} + \mathbf{p}) - E_a^{\text{HF}}(\mathbf{q}, t) - \hbar\omega} - \Pi_a^{\text{RPA}^{\text{R}}}(\mathbf{p}, \omega; t), \quad (58)$$

It is important to realize that this expression (58) con-

where only the Green's function  $g_a^{\text{HF}}$  includes Hartree-Fock self energy contributions. The other Green's functions has an ideal dispersion relation (36). After introduction of relative and center of mass coordinates and a Fourier transform, one obtains

tains more terms than just the first order self energy correction. A Taylor expansion can be performed in order to extract just this first order term in the self energy. Mathematically, the polarization function is a functional with respect to the energy that includes the self energy. Taking the functional derivative with respect to the energy  $E_a(\mathbf{q})$ , we obtain

$$\Pi_a^{\text{SR}}(\mathbf{p}, \omega; t) = \int \frac{d\mathbf{q}}{(2\pi\hbar)^3} \Sigma_a^{\text{HF}}(\mathbf{q}, t) \left\{ \frac{f_a(\mathbf{q} + \mathbf{p}, t) - f_a(\mathbf{q}, t)}{[\hbar\omega + i\epsilon - E_a(\mathbf{q} + \mathbf{p}) + E_a(\mathbf{q})]^2} + \frac{\partial f_a(E_a(\mathbf{q}), t)/\partial E_a(\mathbf{q})}{\hbar\omega + i\epsilon - E_a(\mathbf{q} + \mathbf{p}) + E_a(\mathbf{q})} \right\}. \quad (59)$$

Upon inserting Fermi distribution functions for the transition to equilibrium, we again obtain the same result for the retarded polarization function as DeWitt *et al.* using the Matsubara technique [74]

$$\Pi_a^{\text{SR}}(\mathbf{p}, \omega) = \int \frac{d\mathbf{q}}{(2\pi\hbar)^3} \Sigma_a^{\text{HF}}(\mathbf{q}) \left\{ \frac{f_a(\mathbf{q} + \mathbf{p}) - f_a(\mathbf{q})}{[\hbar\omega + i\epsilon - E_a(\mathbf{q} + \mathbf{p}) + E_a(\mathbf{q})]^2} - \frac{\beta f_a(\mathbf{q})[1 - f_a(\mathbf{q})]}{\hbar\omega + i\epsilon - E_a(\mathbf{q} + \mathbf{p}) + E_a(\mathbf{q})} \right\}. \quad (60)$$


---

Holas *et al.* [66] gave an expression for the self energy term where the first summand of Eq. (60) was missing. It is also prudent to notice that Eqs. (59) & (60) are not well suited for the calculation of the imaginary part of the retarded polarization function. In particular, the square in the denominator of the second summand is usually expanded using the Dirac-Plemelj formula as a derivative of a  $\delta$ -distribution whose evaluation is connected with a number of ambiguities.

## V. RESULTS FOR THE NON-EQUILIBRIUM STRUCTURE

### A. Comparison with results in equilibrium

In order to relate the current calculations to results from the literature, we have to compare to equilibrium data [85]. In equilibrium, exchange, self-energy and correlation contributions can be included into the structure factor and dielectric function in a variety of ways [51, 75–77]. The method presented here, valid in non-equilibrium as well, offers full dynamics in the local field corrections and validity for all degeneracies at the cost of not being able to treat strong correlations. Local field corrections



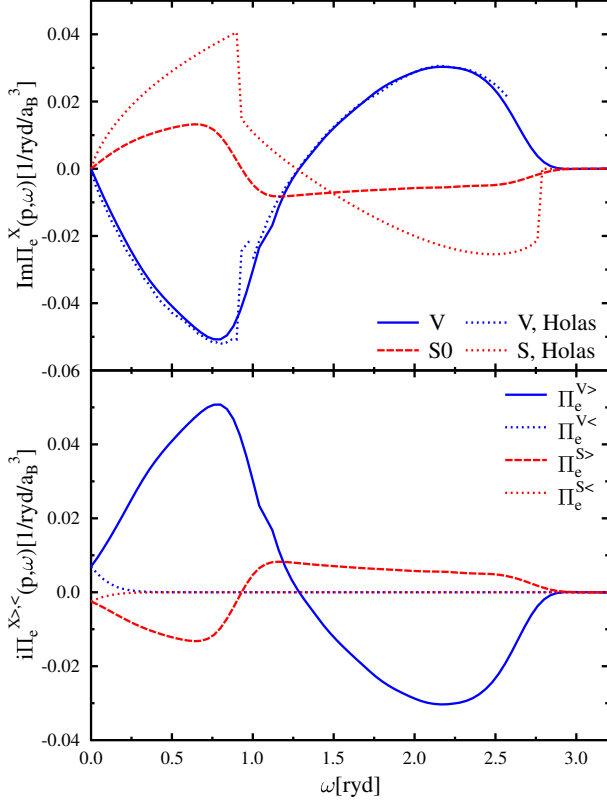


FIG. 1: Results for the vertex (blue lines) and self-energy (red lines) correlation functions (bottom) and the imaginary part of the retarded functions (top) in a degenerate electron gas in equilibrium at  $n_e = 2 \cdot 10^{23} \text{cm}^{-3}$ ,  $T = 0 \text{K}$ ,  $p = 0.964/a_B$ . Current results (solid blue line - vertex, long dashed red line - self energy) are compared to results from Holas *et al.* [66].

accounting for just such strong correlations can be derived for the classical and  $T = 0$ -degenerate limits and in both cases for the  $\omega = 0$  static and  $\omega \rightarrow \infty$  special limits [27, 60, 61, 78]. For intermediate temperatures or arbitrary frequencies, interpolation formulas or expansions are used [47, 49, 51, 62, 79]. Therefore, it is of interest to compare the results of our method with established techniques even though different physical processes are approximated to varying degrees of accuracy within each scheme.

The vertex and self energy terms for a highly degenerate electron gas at  $T = 0$  are shown in Fig. 1. In addition to the imaginary part of the retarded vertex and self energy polarization function corrections, the greater and lesser correlation functions are displayed. There is excellent agreement with data from Holas *et al.* for the vertex term [66]. However, Fig. 1 shows significant deviations between current results for the lowest order self energy term (60) and the result of Holas *et al.* In particular, the discontinuity jumps have vanished and the function is continuous everywhere, even at absolute zero. The con-

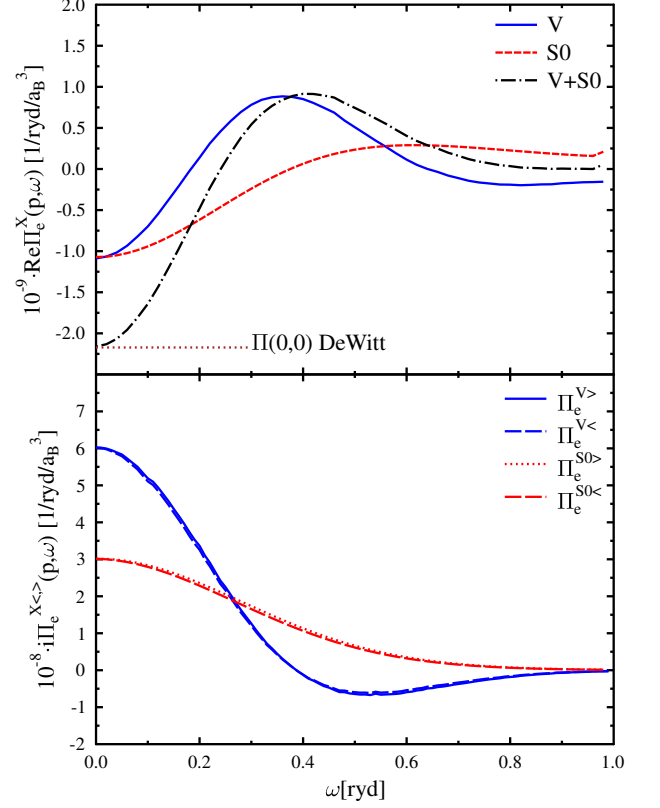


FIG. 2: Results for the vertex (blue lines) and self-energy (red lines) correlation functions (bottom) and the real part of the retarded functions (top) in a non-degenerate electron gas at  $n_e = 10^{21} \text{cm}^{-3}$ ,  $T = 10^6 \text{K}$ ,  $p = 0.1/a_B$  in equilibrium. Current results (solid blue line - vertex, long dashed red line - self energy) are compared to results from DeWitt *et al.* [74].

tinuity of the present calculations and also the difference in the relative amplitudes of the two results are due to the additional term that appears in expression (60) and is missing in Eq. (2.7) of Holas *et al.* [66].

For the case of a non-degenerate electron gas at relatively high temperatures, results are available for the limit of  $\omega \rightarrow 0$  and  $\mathbf{p} \rightarrow 0$  by DeWitt and co-workers [74]. These results are shown in Fig. 2. In particular, the real parts of the retarded self-energy and vertex terms give the same value in the limit of small frequencies and momenta. This behavior is reproduced by our results, which of course give the full frequency and momentum dependence.

The main difference between degenerate and non-degenerate systems to be seen in the vertex and self-energy terms is the apparent small difference between the greater and lesser correlation functions in the non-degenerate case and the large differences in the degenerate case.

The dynamic structure factor of an electron gas and the associated dielectric function  $\varepsilon_{ee}(\mathbf{p}, \omega) = 1 - \Pi_{ee}^R(\mathbf{p}, \omega) V_{ee}(\mathbf{p})$  are shown in Fig. 3. In particular,

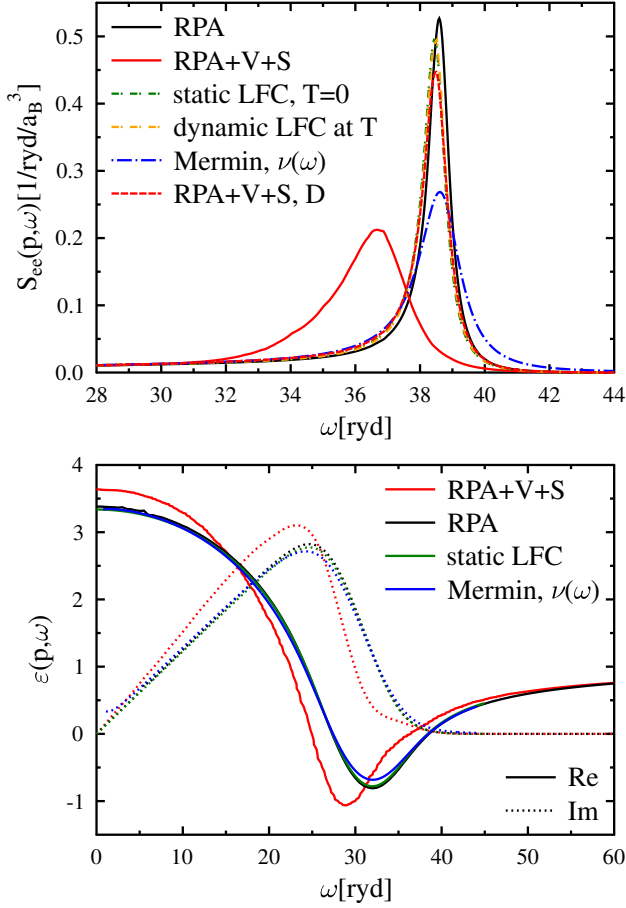


FIG. 3: Results for the dielectric function (bottom) and the structure factor (top) of an electron gas at  $n_e = 10^{26} \text{cm}^{-3}$ ,  $T = 10^6 \text{K}$ ,  $p = 2/a_B$ . The expression for the electron static LFC at  $T = 0$  is fitted from QMC simulations [49, 63]. The dynamic LFC at finite temperatures are derived according to a scheme by Gregori *et al.* [47]. The Mermin dielectric function uses a Born collision frequency [75, 80].

the frequency range around the plasmon peak is displayed. The conditions in this plot correspond to a coupling parameter  $\Gamma_{ee} = 0.32$  and a degeneracy parameter  $n_e \Lambda_e^3 = 41.4$ . As such, there is not a single theory for the structure that is valid in this regime without restriction. As can be seen in Fig. 3, the RPA curve and the curve using static LFC at  $T = 0$  as well as the one using dynamic LFC for the exact temperature, agree well. This ought to indicate that LFC are not very important for this case. However, for the coupling strength in this scenario, RPA cannot be considered a reasonable approximation and deviations from RPA due to electron-electron interactions are expected. Indeed, the structure based on the Mermin dielectric function (using a Born collision frequency) [49, 80] shows a lowering and broadening of the plasmon peak in agreement with the effects of (electron-ion) collisions.

Including the vertex and self energy terms based on

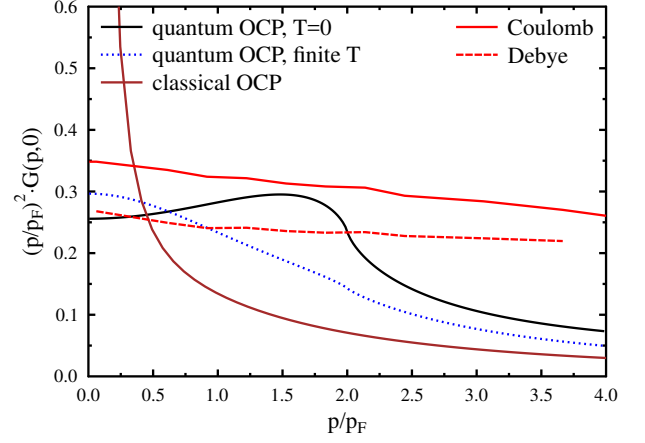


FIG. 4: Results for the static local field corrections (LFC) of an electron gas at  $n_e = 10^{24} \text{cm}^{-3}$ ,  $T = 10^6 \text{K}$ ,  $\Gamma_{ee} = e^2/k_B T d = 0.26$ ,  $n \Lambda_e^3 = 0.41$ . The expression for the electron static LFC at  $T = 0$  is fitted from QMC simulations [63]. The LFC at finite temperatures are derived according to a simple Padé interpolation scheme by Gregori *et al.* [47]. The classical result utilizes the compressibility sum rule [27]. The red curves are obtained using Eq. (28) and the respective potentials in the vertex and self energy terms.

a Coulomb potential changes the plasmon peak considerably in location, height, and width. In this case, electron-electron interactions are solely responsible as direct electron-ion collisions have been neglected. However, evaluating the vertex and self energy terms using a Debye potential (first order in screening) reverts the structure back close to the RPA structure factor. This hints at a cancellation of correlation and screening contributions. However, it can also be argued, that at the present interaction strength it is insufficient to include only the vertex and self energy terms.

We may also extract both static and dynamic LFCs. For example, Fig. 4 shows the static LFC compared to several well-known alternative approaches. Although the magnitude of our result (for both Coulomb and Debye potentials) is of similar magnitude to fits to QMC data [63], the decay of the curves for large momenta is qualitatively different. However, this does not influence the structure much as the static structure tends to unity in any case in this limit. Further, Fig. 4 highlights a general problem: a single theory capable of describing systems with arbitrary degeneracy and strong coupling is not easily to come by. Here, we compare our results that are limited in coupling strength but can handle arbitrary temperatures to a temperature fit between  $T = 0$  QMC results and classical results both of which incorporate arbitrarily strong coupling.

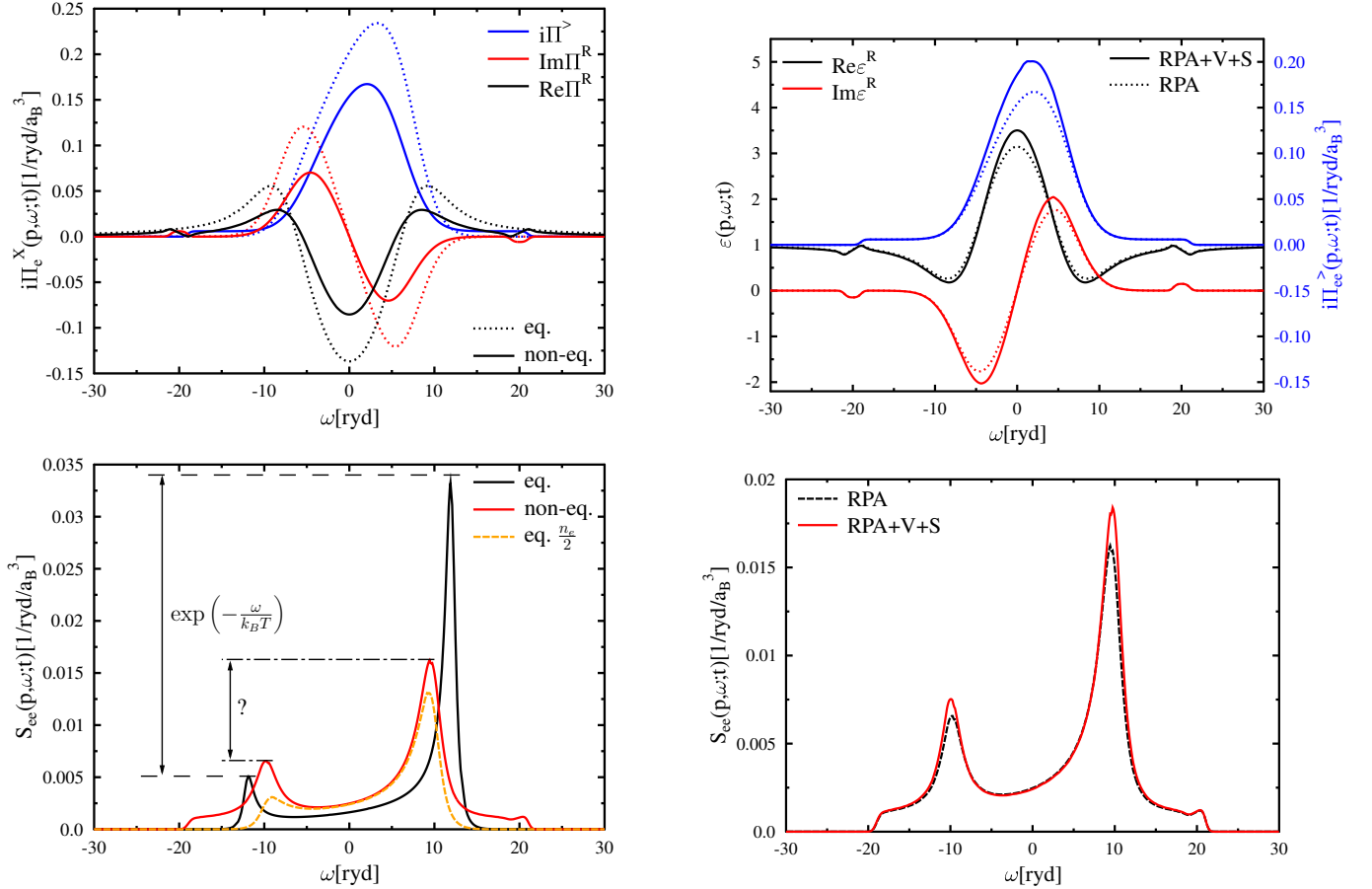


FIG. 5: Structure in an electron gas with  $n_e/2 = 5 \cdot 10^{24}$  at  $T_e = 10^6$ K and the remaining half of the density in a Gaussian bump with  $T_b = 10^4$ K and  $p_b = 10/a_B$ . The momentum is  $p = 1/a_B$ . (Left column) The change in detailed balance due to non-equilibrium effects. (Top) The correlation functions of the polarization function. (Bottom) The electron structure in RPA. The correlation functions obey  $\Pi^>(\mathbf{p}, \omega; t) = \Pi^<(\mathbf{p}, -\omega; t)$ , the imaginary part is odd, the real part of the retarded functions is even. (Right column) The change in the non-equilibrium structure due to the inclusion of vertex and self energy terms. (Top) The real and imaginary parts of the dielectric function and the correlation function of the polarization function  $i\Pi^>$  in RPA and including vertex and self energy. (Bottom) The dynamic structure factor in a non-equilibrium electron gas in RPA and including vertex and self energy corrections.

### B. Non-equilibrium example: Bump-on-hot-tail distribution

For an instructive non-equilibrium example, we consider an electron gas with a density of  $n_e = 10^{25} \text{cm}^{-3}$ , as shown in Fig. 5. The electrons are described by a Wigner distribution function with a bulk electron density of  $n_e/2$  and with the remainder of the electron density contained in a Gaussian bump ( $T_b = 10^4$ K,  $p_b = 10/a_B$ ) produced by, i.e., laser irradiation

$$f_e(p, t) = \left[ \exp\left(\beta \left(\frac{p^2}{2m_e} - \mu_e\right)\right) + 1 \right]^{-1} + C_b \exp(-\beta_b (p - p_b)^2). \quad (61)$$

Here,  $\beta_b = 1/k_B T_b$  is the width of the laser-excited bump. The parameter  $C_b$  is adjusted so that the integration over the bump gives the correct density. The

changes in the different polarization functions are displayed in the top left hand panel of Fig. 5. The general trend is towards a reduction in magnitude of the quantities due to the lower density of electrons in the Fermi-part of the distribution as compared to equilibrium. In addition, the bump in the distribution function causes small features around  $\omega = \pm 20 \text{ryd}$ . The effect of the non-equilibrium distribution function (61) on the DSF of the electron gas are displayed in the bottom left panel of Fig. 5. The plasmon peaks are shifted towards smaller frequencies. Their location, but *not* the height or width, can be well approximated by an equilibrium calculation for half the electron density in this case.

In equilibrium, the ratio of the heights of the plasmon peaks at positive and negative plasmon frequency is given by the detailed balance relation, i.e., the temperature in the system. This is of course not the case in non-

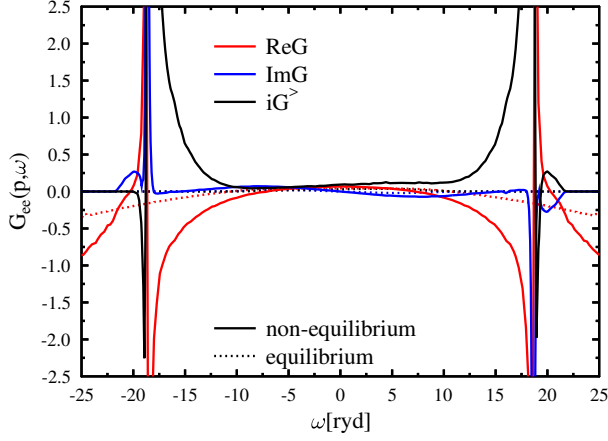


FIG. 6: Dynamic LFC in a non-equilibrium electron gas at parameters as in Fig. 5. The solid lines belong to the non-equilibrium case, the dotted lines are the LFC for the equilibrium case. The momentum is  $p = 1/a_B$ .

equilibrium, where the principle of detailed balance does not apply. In particular, for the chosen conditions, the plasmon peak at positive frequencies is strongly damped while the one at negative frequencies has increased its height. Further, due to the high energy bump in the electron distribution function, the dynamic electron structure features high frequency tails extending to energies beyond the range of the equilibrium structure factor.

Including correlations and exchange does not change the dynamic electron structure in a qualitative way, see the right column in Fig. 5. This is reasonable as the coupling strength is below unity. However, as the vertex and self energy terms increase the magnitude of the dielectric function and the correlation function  $\Pi_{ee}^>$  almost everywhere, the overall effect is very subtle and indeed leads to an increase in the height of the plasmon peaks. This is equivalent to a stiffening of the plasmons, an effect opposite to the usual one observed in equilibrium, where exchange and correlations broaden the quasi-particle resonances (see, e.g., Fig. 3).

The extracted dynamic LFC for the example of Fig. 5 are shown in Fig. 6. The laser energy bump in the distribution function that causes the extra bump in the dynamic structure factor around  $\omega = 20$  is strongly visible in the dynamic LFCs as symmetrically located poles. The real and imaginary parts of the retarded LFC are (anti-)symmetrically, respectively. The larger LFC  $G^>$  is neither.

The full dispersion of all collective excitations for this particular non-equilibrium example is shown in Fig. 7. For small momenta, there exists just one excitation (the plasmon) at a frequency approximately given by the density contained in the Fermi-part of the distribution function, i.e.,  $n_e/2$ . The same is true for the highest momenta shown. The dispersion roughly follows the known quadratic law for small momenta and deviates from it

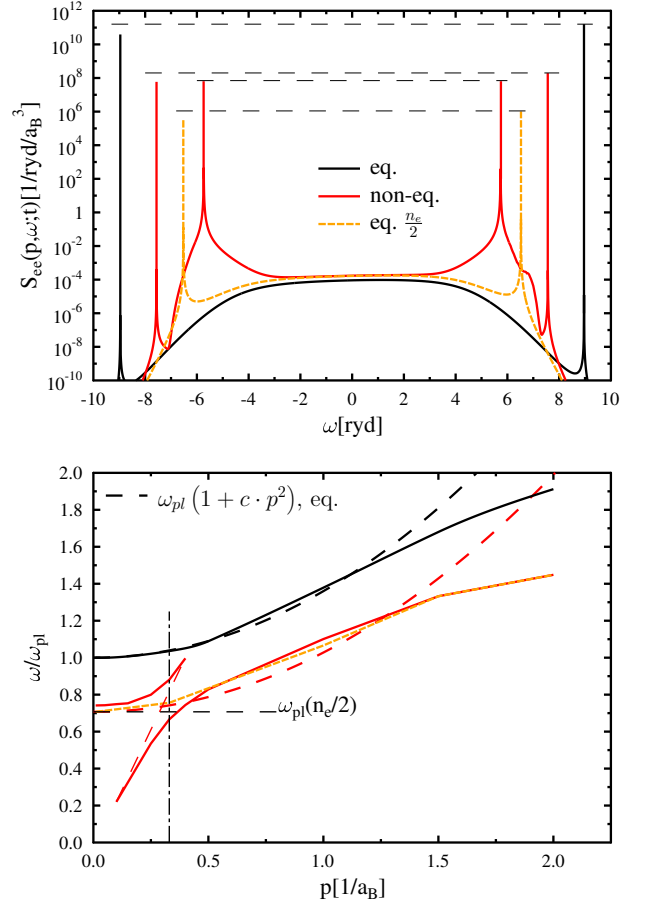


FIG. 7: RPA structure in an electron gas at  $n_e = 10^{25} \text{cm}^{-3}$  in equilibrium at  $T = 10^6 \text{K}$  (black) and in non-equilibrium with  $n_e/2$  at  $T = 10^6 \text{K}$  and  $n_e/2$  in a bump at  $p = 10/a_B$  with a width of  $T_b = 10^4 \text{K}$  (red). (Top panel) The dynamic structure factor is shown for  $p = 0.33/a_B$ , the location of this in the frequency-momentum plane is indicated in the bottom panel with a vertical dash-dotted line. The horizontal lines indicate the detailed balance. For the equilibrium structure factors (solid black and dashed orange lines) it is given by  $\exp(-\omega/k_B T)$ . (Bottom panel) The dispersion relation of longitudinal plasma excitations (the curves are derived from the maximum of the spectral function, not from the zeros of the dielectric function). The fork in the dispersion curve for the non-equilibrium case is due to an interaction of the plasmon and the beam acoustic excitation. The red dashed line is a guide to the eye for the dispersion of an unperturbed acoustic mode (sound speed  $c_s = 3.89 \cdot 10^6 \text{m/s}$ ).

once the damping of the plasmons increases. For momenta from  $p = 0.1/a_B$  to  $p = 0.4/a_B$ , there exist two excitations. The additional one is the beam acoustic mode (BAM) which has been found and described with XRTS for laser driven systems [23, 81–83]. Due to the screening interaction between the plasmon mode and the BAM, mediated by the dielectric function, the dispersion branches do not cross. The plasmon mode gets pushed to higher frequencies and the BAM gets pushed to lower

frequencies. The result is that the upper branch ends up being the BAM excitation even though it was of plasmon character for small momenta. Similarly, the lower mode starts out as BAM but changes character before the upper branch ceases to exist to become the plasmon mode.

The top panel of Fig. 7 shows the detailed balance for a case where the BAM exists. The situation is different to the one described in Fig. 5 where the plasmon peaks of the non-equilibrium system are approximated well by an equilibrium system with half the density. This is due to the occurrence and interaction of plasmon and BAM. Further, whereas plasmon-like modes show asymmetric height, the BAM excitations are symmetrical. In this case, the changes brought on the dynamic structure due to the inclusion of vertex and self energy contributions are not so easily described. Particularly in the frequency range of the BAM, vertex and self energy terms have opposite signs. Therefore, concluding from this example, in a general non-equilibrium situation, the influence of correlations and exchange on damping and location of collective modes cannot be predicted ad hoc, not even qualitatively, but needs to be calculated instead for the specific Wigner distribution function.

## VI. A CHIHARA DECOMPOSITION OF THE TOTAL ELECTRON STRUCTURE FACTOR

The Chihara decomposition of the equilibrium total electron structure factor is the basis for the analysis of experimental x-ray scattering spectra and a cornerstone of interaction between theory and experiment [46, 50, 53, 84]. A similar decomposition into a *free electron* contribution and an *ion* contribution (convolved with the square of screening cloud and form factor) is sought for the general case of non-equilibrium conditions. Such a formalism then allows to rigorously derive simplifications for special cases like two-temperature states or systems with only a single non-equilibrium component.

Naturally, the framework presented in this paper is ideally suited to making rigorous investigations and derivations under non-equilibrium conditions. We start by defining the generalized screening cloud  $\rho(t_1, t_2)$  via the electron-ion and ion-ion correlation functions

$$L_{ei}(t_1, t_2) = \int_C dt_3 \rho(t_1, t_3) L_{ii}(t_3, t_2). \quad (62)$$

From this, after transferring from the Keldysh contour to the physical time axis, enforcing local approximation, and Fourier transforming with respect to the difference variables, the retarded and advanced quantities follow easily

$$L_{ei}^{R/A}(\mathbf{p}, \omega; t) = \rho^{R/A}(\mathbf{p}, \omega; t) L_{ii}^{R/A}(\mathbf{p}, \omega; t). \quad (63)$$

A similar calculation for the related correlation functions

gives the function  $\rho^>$

$$L_{ei}^>(\mathbf{p}, \omega; t) = \rho^>(\mathbf{p}, \omega; t) L_{ii}^A(\mathbf{p}, \omega; t) + \rho^R(\mathbf{p}, \omega; t) L_{ii}^>(\mathbf{p}, \omega; t). \quad (64)$$

We use the Fourier transformed versions of Eqs. (10) and the result for the retarded and advanced generalized screening clouds is

$$\rho^{R/A}(\mathbf{p}, \omega; t) = \frac{\mathcal{Q}_{ei}^{R/A}(\mathbf{p}, \omega; t)}{\mathcal{Q}_{ii}^{R/A}(\mathbf{p}, \omega; t)} \frac{1 - \mathcal{T}_{ii}^{R/A}(\mathbf{p}, \omega; t)}{1 - \mathcal{T}_{ee}^{R/A}(\mathbf{p}, \omega; t)}. \quad (65)$$

From Eqs. (64) & (65), the correlation function for the generalized screening cloud is

$$\begin{aligned} \rho^> = & \frac{1}{|1 - \mathcal{T}_{ee}^R|^2 |\mathcal{Q}_{ii}^R|^2} \left\{ \mathcal{Q}_{ei}^>(1 - \mathcal{T}_{ii}^A) \mathcal{Q}_{ii}^R(1 - \mathcal{T}_{ee}^A) \right. \\ & + \mathcal{Q}_{ei}^A(1 - \mathcal{T}_{ii}^A) \mathcal{Q}_{ii}^R \mathcal{T}_{ee}^> - \mathcal{Q}_{ei}^R(1 - \mathcal{T}_{ii}^A) \mathcal{Q}_{ii}^>(1 - \mathcal{T}_{ee}^A) \\ & \left. - \mathcal{Q}_{ei}^R \mathcal{T}_{ii}^> \mathcal{Q}_{ii}^A(1 - \mathcal{T}_{ee}^A) \right\}, \end{aligned} \quad (66)$$

where all variables  $(\mathbf{p}, \omega; t)$  are again suppressed. Restricting ourselves once again to the DPA, the familiar expressions for the screening clouds can be obtained

$$\rho^{R/A}(\mathbf{p}, \omega; t) = V_{ei}(\mathbf{p}) \mathcal{L}_{ee}^{R/A}(\mathbf{p}, \omega; t), \quad (67)$$

$$\rho^>(\mathbf{p}, \omega; t) = V_{ei}(\mathbf{p}) \mathcal{L}_{ee}^>(\mathbf{p}, \omega; t). \quad (68)$$

Under this approximation, the functions  $\rho^>$  and  $\rho^{R/A}$  describe the usual screening cloud of free electrons in non-equilibrium. In the case of direct electron-ion polarization functions being taken into account as in Eqs. (65) & (66), the screening clouds are generalized to also include the ion form factor as well as bound-free transitions in non-equilibrium. The actual evaluation of the ion form factor or bound-free transitions in non-equilibrium depends on the ability to either solve the screened ladder for the polarization function or to incorporate solutions of the time dependent Schrödinger equation into this formalism.

The Chihara decomposition of the total electron structure factor into free electron part and ion part may be obtained using the generalized ansatz

$$\begin{aligned} L_{ee}(t_1, t_2) = & L_{ee}^{\text{free}}(t_1, t_2) \\ & + \int_C dt_3 dt_4 \rho(t_1, t_3) L_{ii}(t_3, t_4) \rho(t_4, t_2). \end{aligned} \quad (69)$$

As usual, the transfer onto the physical time axis delivers the equation for the correlation functions. The local approximation for the time dependence makes a Fourier transform with respect to the microscopic variables possible. The result is in momentum-frequency space (all functions again depend on the set of variables  $\{\mathbf{p}, \omega, t\}$ )

$$\begin{aligned} L_{ee}^> = & L_{ee}^{\text{free}>} + \rho^> L_{ii}^A \rho^A + \rho^R L_{ii}^> \rho^A + \rho^R L_{ii}^R \rho^>, \\ = & L_{ee}^{\text{free}>} + \rho^> (L_{ei}^A + L_{ei}^R) + |\rho^R|^2 L_{ii}^>. \end{aligned} \quad (70)$$

Here, relation (63) was used to go from the first line to the second line. We can use Eq. (1) to obtain the actual structure factors

$$S_{ee}(\mathbf{p}, \omega; t) = S_{ee}^{\text{free}}(\mathbf{p}, \omega; t) + \frac{i}{\pi} \rho^>(\mathbf{p}, \omega; t) \text{Re} L_{ei}^R(\mathbf{p}, \omega; t) + |\rho^R(\mathbf{p}, \omega; t)|^2 S_{ii}(\mathbf{p}, \omega; t). \quad (71)$$

This is the non-equilibrium generalization of the Chihara formula in the physical (all electron) picture containing the dynamic structure of the free electrons  $S_{ee}^{\text{free}}(\mathbf{p}, \omega; t)$ , the dynamic ion structure  $S_{ii}(\mathbf{p}, \omega; t)$ , and the generalized screening cloud  $\rho^R(\mathbf{p}, \omega; t)$ . In addition, there is a term containing the correlation function  $\rho^>(\mathbf{p}, \omega; t)$  and the electron-ion retarded density fluctuation correlation function  $L_{ei}^R(\mathbf{p}, \omega; t)$ . The latter term vanishes in equilibrium once the Born-Oppenheimer approximation separating the electron and ion energy scales is applied and the screening cloud is taken at  $\omega = 0$ . In equilibrium,  $\rho^>$  is related to the imaginary part of the retarded screening cloud  $\rho^R$  which vanishes for  $\omega = 0$ .

The Chihara decomposition for the retarded and advanced quantities reads

$$L_{ee}^{R/A}(\mathbf{p}, \omega; t) = L_{ee}^{\text{free}R/A}(\mathbf{p}, \omega; t) + \rho^{R/A}(\mathbf{p}, \omega; t) L_{ii}^{R/A}(\mathbf{p}, \omega; t) \rho^{R/A}(\mathbf{p}, \omega; t). \quad (72)$$

From the known expressions for the generalized screening cloud and the ion-ion and electron-ion structure, the retarded/advanced structure of the free electron gas can be obtained as

$$L_{ee}^{\text{free}R/A} = \frac{1}{Q_{ii}^{R/A} (1 - \mathcal{T}_{ee}^{R/A})^2} \times \left\{ Q_{ee}^{R/A} Q_{ii}^{R/A} (1 - \mathcal{T}_{ee}^{R/A}) - (Q_{ei}^{R/A})^2 (1 - \mathcal{T}_{ii}^{R/A}) \right\}. \quad (73)$$

Again, the dependence on  $(\mathbf{p}, \omega; t)$  was suppressed. This complicated structure reflects that the gas of “free” electrons considered here exists in a correlated system containing ions and other electrons. For the case of the DPA, this reduces to

$$L_{ee}^{\text{free}R/A}(\mathbf{p}, \omega; t) = \mathcal{L}_{ee}^{R/A}(\mathbf{p}, \omega; t), \quad (74)$$

as expected. The calculation of the correlation function for the density response of the free electron gas is rather lengthy but straightforward and one obtains

$$L_{ee}^{\text{free} >} = \frac{1}{|1 - \mathcal{T}_{ee}^R|^4 |Q_{ii}^R|^2} \left\{ |1 - \mathcal{T}_{ee}^R|^2 |Q_{ii}^R|^2 [\mathcal{Q}_{ee}^> (1 - \mathcal{T}_{ee}^A) + Q_{ee}^A \mathcal{T}_{ee}^>] - \mathcal{Q}_{ei}^> Q_{ei}^A (1 - \mathcal{T}_{ii}^A) Q_{ii}^R |1 - \mathcal{T}_{ee}^R|^2 \right. \\ - \mathcal{Q}_{ei}^> Q_{ei}^R (1 - \mathcal{T}_{ii}^A) Q_{ii}^R (1 - \mathcal{T}_{ee}^A)^2 - Q_{ei}^A{}^2 (1 - \mathcal{T}_{ii}^A) Q_{ii}^R \mathcal{T}_{ee}^> (1 - \mathcal{T}_{ee}^R) \\ - |Q_{ei}^R|^2 (1 - \mathcal{T}_{ii}^A) Q_{ii}^R \mathcal{T}_{ee}^> (1 - \mathcal{T}_{ee}^A) + Q_{ei}^A{}^2 (1 - \mathcal{T}_{ii}^A) Q_{ii}^> (1 - \mathcal{T}_{ee}^A)^2 \\ \left. + Q_{ei}^R{}^2 \mathcal{T}_{ii}^> Q_{ii}^A (1 - \mathcal{T}_{ee}^A)^2 \right\}. \quad (75)$$

This greatly simplifies in DPA to

$$L_{ee}^{\text{free} >}(\mathbf{p}, \omega; t) = \mathcal{L}_{ee}^>(\mathbf{p}, \omega; t). \quad (76)$$

The degree of complexity underpinning the structure of the free electron gas found in Eqs. (73) & (75) is a reflection of the fact that the cross species contributions to the polarization functions allow for a vastly wider range of routes for density excitations to couple. It is therefore worth stating that a great deal of interesting and complicated physics may have been neglected in the analysis of XRTS data since the high-frequency electronic response is ubiquitously approximated as that of a pure electron gas.

#### A. Example for the Chihara decomposition in non-equilibrium

As an example for a two-component material, we consider hydrogen at a total proton density of  $n_p = 10^{26} \text{cm}^{-3}$ , as shown in Fig. 8. The ions (protons) are in equilibrium at a temperature of  $T = 10^6 \text{K}$ . The electrons are described by a Wigner distribution function with a bulk electron density of  $n_e = 10^{24} \text{cm}^{-3}$  and with the remainder of the electron density contained in a Gaussian bump ( $T_b = 10^4 \text{K}$ ,  $p_b = 8/a_B$ ). The top-right hand panel in Fig. 8 shows the differences in the correlation functions of the polarization function between equilibrium and non-equilibrium. The magnitude of the non-equilibrium functions is smaller because of the reduced

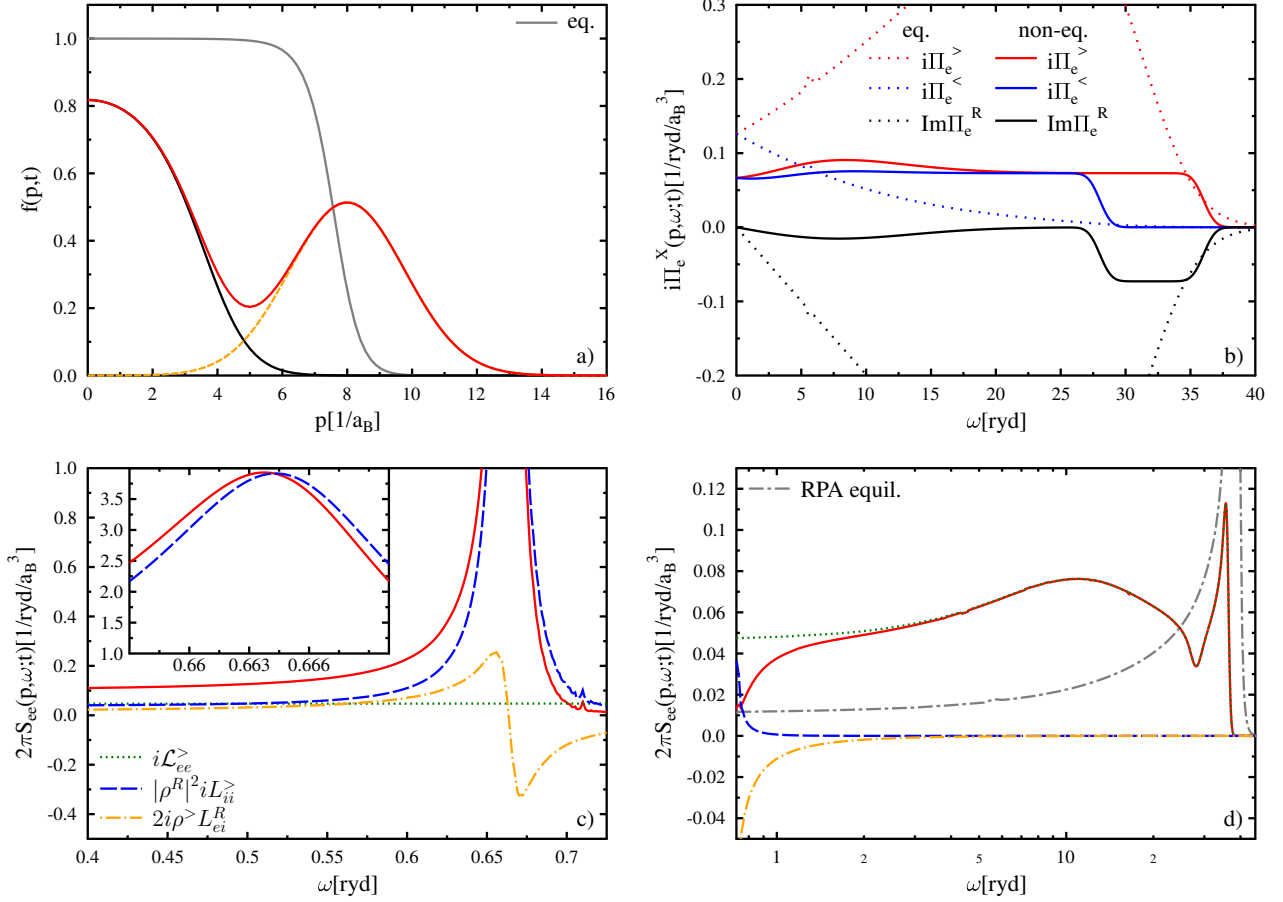


FIG. 8: Total electron structure factor in RPA in non-equilibrium dense hydrogen and its Chihara decomposition for a wave number of  $p = 2/a_B$ . a) Wigner distribution functions for a total electron density of  $n_e = 10^{26} \text{ cm}^{-3}$ . Equilibrium distribution for  $T = 10^6 \text{ K}$  (solid grey line, used for the protons), equilibrium distribution for  $n_e = 10^{24} \text{ cm}^{-3}$ ,  $T = 10^6 \text{ K}$  (solid black line), Gaussian bump centered at  $p = 8/a_B$  with  $\beta_b = 1/k_B/10^4 \text{ K}$  (dashed orange line). The actually used non-equilibrium distribution for the electrons is the solid red line. b) Correlation functions and the imaginary part of the retarded polarization function. c) Proton dominated part of the electron structure factor. The free electron contribution is the dotted green line, the proton structure convoluted with the screening cloud is the dashed blue line, the electron-ion mix term is given by the dash-dotted orange line, and the total electron structure factor is the solid red line. The inset shows the ion acoustic peak in detail. d) Electron dominated part of the total electron structure factor. Beware, the x-axis has a logarithmic scale. The labeling of the curves is the same as in panel c). For comparison the structure factor for an equilibrium system at the same density is shown (corresponding to the equilibrium distribution function in panel a)).

bulk density. The extension in frequency space is comparable with the equilibrium case due to the high energy bump in the distribution function. The bottom row of Fig. 8 displays the ion acoustic mode (left panel) and the electron part (right panel) of the total electron structure factor. The ion acoustic mode is exceptionally well developed due to the non-equilibrium in the electron subsystem and the corresponding changes in the electronic screening of the ion-ion interactions. It can further be seen, that the full ion acoustic peak is dominated by the total ion structure factor  $iL_{ii}^>$  multiplied by the non-equilibrium electron screening cloud  $|\rho^R|^2$ . Nevertheless, the non-equilibrium free electron gas structure  $i\mathcal{L}_{ee}^>$  and the electron-ion mix term  $i2\rho^>\text{Re}L_{ei}^R$  give important con-

tributions which are of the same order. This is a special attribute which appears only for non-equilibrium distribution functions as the latter term vanishes in equilibrium due to the scale separation of electrons and ions which, again only in equilibrium, gives rise to the application of the Born-Oppenheimer approximation. The electron part of the total electron structure factor is given to high accuracy by the free electron structure factor  $i\mathcal{L}_{ee}^>$ . The deviation from equilibrium is visible in the reduced height of the plasmon feature at  $\omega \sim 35 \text{ ryd}$  and in the broad feature with a second maximum to the left of the plasmon peak.



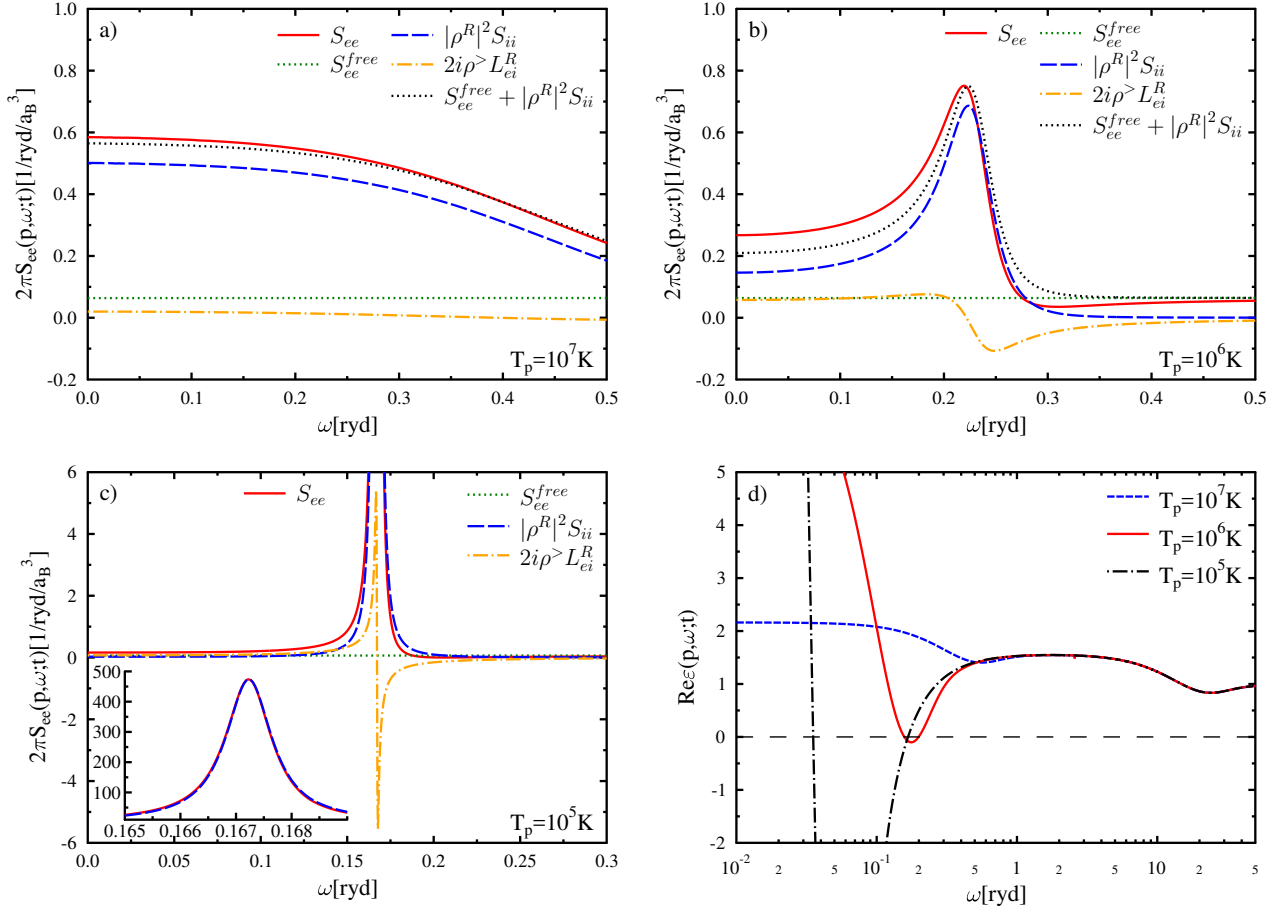


FIG. 9: Proton acoustic mode part of the total electron structure factor in RPA in two-temperature dense hydrogen and it's Chihara decomposition for a total electron density of  $n_e = 10^{25} \text{cm}^{-3}$  and a wave number of  $p = 1/a_B$ . The electron temperature is always  $T_e = 10^7 \text{K}$ . The proton temperature changes from  $T_p = 10^7 \text{K}$  (equilibrium, panel a)), to  $T_p = 10^6 \text{K}$  (panel b)), and  $T_p = 10^5 \text{K}$  (panel c)). The inset in panel c) shows the ion peak in more detail. Panel d) contains the real part of the full hydrogen dielectric function for these three temperatures demonstrating the appearance of zeros and therefore of the ion acoustic mode.

### B. Chihara decomposition in a two-temperature systems

During the relaxation process, there is usually a time span during which the non-equilibrium system may be modeled as a two-temperature system with a temperature ascribed to the electron subsystem and a different temperature to the ion subsystem. Such states have been found in experiments to last for up to several hundred picoseconds and the general agreement in the description of the energy transfer and relaxation process between theory and experiment is not at an acceptable level currently [9, 10, 18]. XRTS has emerged as a possible diagnostics for such relaxation, shedding light on the time scales and mechanisms [18]. The underlying theory for the electronic structure naturally needs to capture the non-equilibrium physics adequately. Figure 9 demonstrates that the current formalism of this paper is well suited to describe two-temperature systems and

that a description using an equilibrium structure theory will introduce errors. In equilibrium, (Fig. 9, panel a) there is no problem with the decomposition of the total electron structure factor into free electron part and ion part. With a reduction of the ion temperature in relation to the electron temperature and under proper coupling of the ion density modes and the electron screening, a screened ion acoustic mode forms (Fig. 9, panel d, zeros of the real part of the dielectric function, black curve). Once this is the case, the electron-ion cross term in the Chihara formula, comprised of the correlation function of the electron screening cloud and the electron-ion structure, does not vanish anymore and is of the same order as the free electron feature in the spectral range of the ion acoustic mode. This constitutes a breakdown of the Born-Oppenheimer approximation, on which the usual equilibrium Chihara decomposition is founded. For very large temperature differences however, it seems to be the case that the *relative* error introduced by neglecting the



$i2\rho^>\text{Re}L_{ei}^R$  term is tolerable. However, as large temperature differences between species often occur at the beginning of the relaxation process where it is most likely that either one or even both species have not yet fully established their own temperature, it seems prudent to always use the full non-equilibrium formalism.

## VII. SUMMARY

The paper presents the theory needed to calculate the dynamic structure in a quantum correlated two-component non-equilibrium system. The theory for the dynamic structure includes, technically, all interactions. The realization of the theory does however depend on the approximation for the polarization function and the Wigner distribution functions. Still a most general framework of equations has been provided. Specific cases like the two fluid approximation, in which the electron-ion polarization function is neglected, have been discussed. The latter leads to results that agree with published results for the energy transfer rate and the structure factor.

A scheme is presented to introduce local field corrections to non-equilibrium systems with small coupling between the species. At this stage such formalism seems largely academic as it is not needed if correlations and exchange are included via the polarization functions. However, strong correlations are unlikely to be included successfully using a perturbation expansion of the polarization function as showcased in this paper. Therefore, such LFC scheme could be of use for non-equilibrium systems as well, if a closure relation can be found.

The considered exchange and correlation corrections to the RPA polarization function are the vertex term and first self energy contributions. The equilibrium expressions for these terms have been known for a long time, its non-equilibrium generalizations, in particular the correlation functions, have first been presented here. Comparison of the vertex and self energy terms with literature values for equilibrium situations shows good agreement in the non-degenerate limit. In the  $T=0$  limit, the vertex term is computed in agreement with known results. However, the self energy term as calculated here, is a generalization of published results. It is important to point out that the current numerical implementation of vertex and self energy terms is capable of delivering frequency and momentum dependent polarization functions at any degeneracy in equilibrium and non-equilibrium. The same is then of course true for the dynamic structure factor.

For specific results, Wigner distribution functions for electrons and ions are needed as input quantities. In equilibrium, the difference between screened and unscreened polarization function corrections has been demonstrated. In general, exchange and correlation contributions have the expected effect of broadening and shifting quasi-particle excitations. The current corrections to RPA do agree with known LFC in specific limits but large deviations

can be expected in general.

Typical examples of Wigner distribution functions have been used to demonstrate non-equilibrium effects. For laser driven electrons in a model electron gas, the change in the total electron structure was shown. This includes the change in plasmon position and width, and the change in the non-equilibrium detailed balance. For the specific non-equilibrium example shown, a stiffening of the plasmon resonance can be observed. This points out that, in non-equilibrium situations, the effect of exchange and correlation cannot be predicted ad hoc. The dispersion relation shows the formation of a BAM, one of many possible driven collective excitations in non-equilibrium. These interact in a complicated way with the plasmons.

A generalized non-equilibrium electronic screening cloud, i.e. a non-equilibrium form factor, has been introduced. This enables a Chihara-like decomposition of the total electron structure into a free electron part and a part describing the electrons associated with the ion structure, be it as bound electrons or as screening cloud. Such decomposition cannot and does not rely on the Born-Oppenheimer approximation in non-equilibrium and additional terms to the equilibrium decomposition arise due to this feature. Such non-equilibrium decomposition will be of use for experiments trying to create and probe matter on femto-second time scales using ultra-short lasers, XFELs, and XRTS.

The example for laser-driven electrons in warm dense hydrogen shows the non-equilibrium coupling of the electrons to the ions. This leads to an asymmetric change in the peak of the ion acoustic mode. The electron-ion cross term is of similar order as the free electron feature for ion excitation frequencies. The free electron part of the total electron structure is given to high accuracy by the free electron structure.

For two-temperature systems, it was shown that an equilibrium treatment using two different temperatures should be used only for very small temperature differences. For most situations, electron-ion cross terms play a role that cannot be neglected.

The current work offers many possibilities and challenges for future work. It gives a framework for more general energy transfer rates. The coupling of micro- and macro-variables needs to be studied in order to take into account gradients. In order to treat strong correlations, closure relations for the LFCs in non-equilibrium would be needed urgently. In addition, the electron-ion polarization function, or more generally speaking the electron-ion problem, should be studied in non-equilibrium.

## Acknowledgments

The authors gratefully acknowledge fruitful discussions with and comments from D.O. Gericke (University of Warwick). J.V. also acknowledges generous hospitality at SIMES, SLAC, Stanford (USA).

This document is of United Kingdom origin and con-

tains proprietary information which is the property of the Secretary of State for Defence. It is furnished in confidence and may not be copied, used or disclosed in whole

or in part without prior written consent of Defence Intellectual Property Rights DGDCDIPR-PL - Ministry of Defence, Abbey Wood, Bristol, BS34 8JH, England

- 
- [1] S. H. Glenzer and R. Redmer, *Rev. Mod. Phys.* **81**, 1625 (2009).
  - [2] S. H. Glenzer, B. J. MacGowan, P. Michel, N. B. Meezan, L. J. Suter, S. N. Dixit, J. L. Kline, G. A. Kyrala, D. K. Bradley, D. A. Callahan, et al., *Science* **327**, 1228 (2010).
  - [3] L. B. Fletcher, H. J. Lee, T. Döppner, M. Galtier, B. Nagler, P. Heimann, C. Fortmann, S. LePape, T. Ma, M. Millot, et al., *Nature Photonics* **9**, 274 (2015).
  - [4] M. D. Knudson, M. P. Desjarlais, A. Becker, R. W. Lemke, K. R. Cochrane, M. E. Savage, D. E. Bliss, T. R. Mattson, and R. Redmer, *Science* **348**, 1455 (2015).
  - [5] D. Bäuerle, *Laser Processing and Chemistry* (Springer Verlag, Berlin, Heidelberg, 2011).
  - [6] P. Balling and J. Schou, *Reports on Progress in Physics* **76**, 036502 (2013).
  - [7] A. Vogel and V. Venugopalan, *Chem. Rev.* **103**, 577 (2003).
  - [8] C. Frischkorn and M. Wolf, *Chem. Rev.* **106**, 4207 (2006).
  - [9] P. Celliers, A. Ng, G. Xu, and A. Forsman, *Phys. Rev. Lett.* **68**, 2305 (1992).
  - [10] A. Ng, P. Celliers, G. Xu, and A. Forsman, *Phys. Rev. E* **52**, 4299 (1995).
  - [11] H. J. Lee, P. Neumayer, J. Castor, T. Döppner, R. W. Falcone, C. Fortmann, B. A. Hammel, A. L. Kritcher, O. L. Landen, R. W. Lee, et al., *Phys. Rev. Lett.* **102**, 115001 (2009).
  - [12] W. S. Fann, R. Storz, H. W. K. Tom, and J. Bokor, *Phys. Rev. B* **46**, 13592 (1992).
  - [13] R. H. M. Groeneveld, R. Sprik, and A. Lagendijk, *Phys. Rev. B* **51**, 11433 (1995).
  - [14] R. Knorren, K. H. Bennemann, R. Burgermeister, and M. Aeschlimann, *Phys. Rev. B* **61**, 9427 (2000).
  - [15] R. Ernstorfer, M. Harb, C. T. Hebeisen, G. Sciaini, T. Dartigalongue, and R. J. D. Miller, *Science* **323**, 1033 (2009).
  - [16] L. Waldecker, R. Berton, R. Ernstorfer, and J. Vorberger, to be published (2015).
  - [17] R. R. Fäustlin, T. Bornath, T. Döppner, S. Düsterer, E. Förster, C. Fortmann, S. H. Glenzer, S. Göde, G. Gregori, R. Irsig, et al., *Phys. Rev. Lett.* **104**, 125002 (2010).
  - [18] T. G. White, J. Vorberger, C. R. D. Brown, B. J. B. Crowley, P. Davis, S. H. Glenzer, J. W. O. Harris, D. C. Hochhaus, S. LePape, T. Ma, et al., *Scientific Rep.* **2**, 889 (2012).
  - [19] D. Kremp, T. Bornath, M. Bonitz, and M. Schlanges, *Phys. Rev. E* **60**, 4725 (1999).
  - [20] N.-H. Kwong and M. Bonitz, *Phys. Rev. Lett.* **84**, 1768 (2000).
  - [21] A. Kaiser, B. Rethfeld, M. Vicanek, and G. Simon, *Phys. Rev. B* **61**, 11437 (2000).
  - [22] B. Rethfeld, A. Kaiser, M. Vicanek, and G. Simon, *Phys. Rev. B* **65**, 214303 (2002).
  - [23] D. A. Chapman and D. O. Gericke, *Phys. Rev. Lett.* **107**, 165004 (2011).
  - [24] N. Medvedev, U. Zastra, E. Förster, D. O. Gericke, and B. Rethfeld, *Phys. Rev. Lett.* **107**, 165003 (2011).
  - [25] B. Y. Müller and B. Rethfeld, *Phys. Rev. B* **87**, 035139 (2013).
  - [26] N. Medvedev, Z. Li, and B. Ziaja, *Phys. Rev. B* **91**, 054113 (2015).
  - [27] D. Kremp, M. Schlanges, and W.-D. Kraeft, *Quantum statistics of nonideal plasmas* (Springer Verlag, Berlin, Heidelberg, 2005).
  - [28] D. Semkat, D. Kremp, and M. Bonitz, *Phys. Rev. E* **59**, 1557 (1999).
  - [29] M. Schlanges, T. Bornath, and D. Kremp, *Phys. Rev. A* **38**, 2174 (1988).
  - [30] T. Bornath, M. Schlanges, and R. Prenzel, *Physics of Plasmas* **5**, 1485 (1998).
  - [31] S. M. Vinko, O. Ciricosta, T. R. Preston, D. S. Rackstraw, C. R. D. Brown, T. Burian, J. Chalupsky, B. I. Cho, H.-K. Chung, K. Engelhorn, et al., *Nature Comm.* **6**, 6397 (2015).
  - [32] J. Vorberger, D. O. Gericke, T. Bornath, and M. Schlanges, *Phys. Rev. E* **81**, 046404 (2010).
  - [33] E. Galtier, F. B. Rosmej, T. Dzelzainis, D. Riley, F. Y. Khattak, P. Heimann, R. W. Lee, A. J. Nelson, S. M. Vinko, T. Whitcher, et al., *Chem. Rev.* **106**, 164801 (2011).
  - [34] S. P. Hau-Riege, A. Graf, T. Döppner, R. A. London, J. Krzywinski, C. Fortmann, S. H. Glenzer, M. Frank, K. Sokolowski-Tinten, M. Messerschmidt, et al., *Phys. Rev. Lett.* **108**, 217402 (2012).
  - [35] U. Zastra, P. Sperling, M. Harmand, A. Becker, T. Bornath, R. Bredow, S. Dziarzhyski, T. Fennel, L. B. Fletcher, E. Förster, et al., *Phys. Rev. Lett.* **112**, 105002 (2014).
  - [36] S. H. Glenzer, O. L. Landen, P. Neumayer, R. W. Lee, K. Widmann, S. W. Pollaine, R. J. Wallace, G. Gregori, A. Höll, T. Bornath, et al., *Phys. Rev. Lett.* **98**, 065002 (2007).
  - [37] E. Garcia Saiz, G. Gregori, D. O. Gericke, J. Vorberger, B. Barbrel, R. J. Clarke, R. R. Freeman, S. H. Glenzer, F. Y. Khattak, M. Koenig, et al., *Nature Physics* **4**, 940 (2008).
  - [38] A. L. Kritcher, P. Neumayer, J. Castor, T. Döppner, R. W. Falcone, O. L. Landen, R. W. Hae, J. L. and Lee, E. C. Morse, A. Ng, S. Pollaine, et al., *Science* **322**, 69 (2008).
  - [39] S. P. Regan, K. Falk, G. Gregori, P. B. Radha, S. X. Hu, T. R. Boehly, B. J. B. Crowley, S. H. Glenzer, O. L. Landen, D. O. Gericke, et al., *Phys. Rev. Lett.* **109**, 265003 (2012).
  - [40] T. Ma, T. Döppner, R. W. Falcone, L. Fletcher, C. Fortmann, D. O. Gericke, O. L. Landen, H. J. Lee, A. Pak, J. Vorberger, et al., *Phys. Rev. Lett.* **110**, 065001 (2013).
  - [41] D. Kraus, J. Vorberger, D. O. Gericke, V. Bagnoud, A. Blažević, W. Cayzac, A. Frank, G. Gregori, A. Otten, et al., *Phys. Rev. Lett.* **111**, 255501 (2013).
  - [42] D. A. Chapman, J. Vorberger, L. B. Fletcher, R. A. Baggot, L. Divol, T. Döppner, R. W. Falcone, S. H. Glenzer, G. Gregori, T. M. Guymer, et al., *Nature Comm.* **6**, 6839 (2015).

- (2014).
- [43] N. Hartley, P. Belancourt, D. Chapman, T. Dppner, R. Drake, D. Gericke, S. Glenzer, D. Khaghani, S. LePape, T. Ma, et al., *High Energy Density Physics* **14**, 1 (2015), ISSN 1574-1818.
  - [44] M. W. C. Dharma-wardana and F. Perrot, *Phys. Rev. E* **58**, 3705 (1998).
  - [45] S. B. Hansen and A. S. Shlyaptseva, *Phys. Rev. E* **70**, 036402 (2004).
  - [46] J. Chihara, *J. Phys. Cond. Matt.* **12**, 231 (2000).
  - [47] G. Gregori, A. Ravasio, A. Höll, S. H. Glenzer, and S. J. Rose, *High Energy Dens. Phys.* **3**, 99 (2007).
  - [48] K. Wünsch, J. Vorberger, and D. O. Gericke, *Phys. Rev. E* **79**, 010201(R) (2009).
  - [49] C. Fortmann, A. Wierling, and G. Röpke, *Phys. Rev. E* **81**, 026405 (2010).
  - [50] K. Wünsch, J. Vorberger, G. Gregori, and D. O. Gericke, *Europhys. Lett.* **94**, 25001 (2011).
  - [51] J. Vorberger and D. O. Gericke, *High Energy Density Phys.* **9**, 178 (2013).
  - [52] J. Vorberger, Z. Donko, I. M. Tkachenko, and D. O. Gericke, *Phys. Rev. Lett.* **109**, 225001 (2012).
  - [53] J. Vorberger and D. O. Gericke, *Phys. Rev. E* **91**, 033112 (2015).
  - [54] K.-U. Plagemann, H. R. Rüter, T. Bornath, M. Shihab, M. P. Desjarlais, C. Fortmann, S. H. Glenzer, and R. Redmer, *Phys. Rev. E* **92**, 013103 (2015).
  - [55] D. A. Chapman, J. Vorberger, K. Wünsch, and D. O. Gericke, *High Energy Density Phys.* **8**, 175 (2012).
  - [56] D. Pines and F. Noziere, *Theory of quantum liquids* (Benjamin, New York, 1966).
  - [57] V. L. Keldysh, *Sov. Phys. JETP* **20**, 235 (1965).
  - [58] D. C. Langreth and J. W. Wilkins, *Phys. Rev. B* **6**, 3189 (1972).
  - [59] J. Vorberger and D. O. Gericke, *Phys. Plasma* **16**, 082702 (2009).
  - [60] K. S. Singwi, M. P. Tosi, R. H. Land, and A. Sjölander, *Phys. Rev.* **176**, 589 (1968).
  - [61] N. Iwamoto, *Phys. Rev. A* **30**, 3289 (1984).
  - [62] J. Hong and C. Kim, *Phys. Rev. A* **43**, 1965 (1991).
  - [63] B. Farid, V. Heine, G. E. Engel, and I. J. Robertson, *Phys. Rev. B* **48**, 11602 (1993).
  - [64] D. J. W. Geldart and R. Taylor, *Can. Journal Phys.* **48**, 155 (1970).
  - [65] D. J. W. Geldart and R. Taylor, *Can. Journal Phys.* **48**, 167 (1970).
  - [66] A. Holas, P. K. Aravind, and K. S. Singwi, *Phys. Rev. B* **20**, 4912 (1979).
  - [67] F. Green, D. Neilson, and J. Szymanski, *Phys. Rev. B* **31**, 2779 (1985).
  - [68] R. Cenni and P. Saracco, *Nuclear Phys.* **A487**, 279 (1988).
  - [69] E. Engel and S. H. Vosko, *Phys. Rev. B* **42**, 4940 (1990).
  - [70] H. O. Frota and G. D. Mahan, *Phys. Rev. B* **45**, 6243 (1992).
  - [71] C. F. Richardson and N. W. Ashcroft, *Phys. Rev. B* **50**, 8170 (1994).
  - [72] M. Hindgren and C.-O. Almbladh, *Phys. Rev. B* **56**, 12832 (1997).
  - [73] J. Vorberger, M. Schlages, and W. D. Kraeft, *Phys. Rev. E* **69**, 046407 (2004).
  - [74] H. E. DeWitt, M. Schlages, A. Y. Sakakura, and W. D. Kraeft, *Phys. Lett. A* **197**, 326 (1995).
  - [75] H. Reinholz, R. Redmer, G. Röpke, and A. Wierling, *Phys. Rev. E* **62**, 5648 (2000).
  - [76] Y. V. Arkhipov, A. Askaruly, D. Ballester, A. E. Davletov, I. M. Tkachenko, and G. Zwicknagel, *Phys. Rev. E* **81**, 026402 (2010).
  - [77] J. P. Mithen, J. Daligault, and G. Gregori, *Phys. Rev. E* **85**, 056407 (2012).
  - [78] G. D. Mahan, *Many particle physics* (Plenum Press, New York, 1990).
  - [79] B. Dabrowski, *Phys. Rev. B* **34**, 4989 (1986).
  - [80] N. D. Mermin, *Phys. Rev. B* **1**, 2362 (1970).
  - [81] T. M. O'Neil and J. H. Malmberg, *Physics of Fluids* **11**, 1754 (1968).
  - [82] J. L. Kline, D. S. Montgomery, B. Bezzerides, J. A. Cobble, D. F. DuBois, R. P. Johnson, H. A. Rose, L. Yin, and H. X. Vu, *Phys. Rev. Lett.* **94**, 175003 (2005).
  - [83] H. X. Vu, L. Yin, D. F. DuBois, B. Bezzerides, and E. S. Dodd, *Phys. Rev. Lett.* **95**, 245003 (2005).
  - [84] J. Chihara, *Journal of Physics F: Metal Physics* **17**, 295 (1987).
  - [85] We perform all our calculations in Heaviside units  $4\pi\epsilon_0 = \hbar = c^2 = 2m_e = 1$ , energies are in Rydberg, momenta in  $1/a_B$ .